UNIVERSITAT POLITÈCNICA DE CATALUNYA
BARCELONATECH
Escola Tècnica Superior d'Enginyeria
de Telecomunicació de Barcelona

telecos
BCN

Design and validation of current probes for studying RF current flux through mechanical aircraft joints

Master Thesis
submitted to the Faculty of the
Escola Tècnica d'Enginyeria de Telecomunicació de Barcelona
Universitat Politècnica de Catalunya
by

Jordi Solé Lloveras

In partial fulfillment
of the requirements for the master in
MASTER IN ELECTRONIC ENGINEERING

Advisor: Ferran Silva
Barcelona, June 2022

telecos
BCN

Contents

List of Figures

List of Tables

Revision history and approval record

Revision	Date	Purpose
0	09/02/2022	Document creation
1	20/06/2022	Document revision

DOCUMENT DISTRIBUTION LIST

Name	e-mail
Jordi Solé Lloveras	jordi.sole.lloveras@upc.edu
Ferran Silva	ferran.silva@upc.edu

Written by:		Reviewed and approved by:	
Date	17/06/2022	Date	20/06/202
Name	Jordi Solé Lloveras	Name	Ferran Silva
Position	Project Author	Position	Project Supervisor

Abstract

The study of electrical currents flowing through the airframe is very important from an EMC (Electromagnetic Compatibility) standpoint due to the potential to produce severe aircraft faults. As an example, direct lightning strikes are one of the main failure causes, effect on which we will orient our work. Furthermore, one of the key points where the study of currents is more complex are the discontinuities formed by the mechanical joints that attach fuselage plates, in addition to the difficulty of placing sensors to measure current flowing through these junctions.

In this work, a fixture intended to emulate such discontinuities of mechanically attached panels will be developed and evaluated. Subsequently, a prototype of probes capable to measure current flow will be built and studied theoretically and experimentally. Having the prototypes validated, flat probes embedded in a PCB will be constructed to be able to be inserted into the mechanical junctions, such as screws or rivets. Finally, current probes will be verified by means of a surge generator, capable of producing a wave similar to the one originated by a direct lightning strike.

1 Introduction

1.1 Statement of purpose

Electromagnetic interference (EMI) is a very common reason which causes many types of electronic devices to act in an unexpected way. The effects can range from minor annoyances to the user (e.g. our PC display flickering) to fatal accidents due to an error in a critical safety system (such as a vehicle's brakes).

It is important to consider a set of good engineering practices when designing electronic devices to avoid all these problems. Electromagnetic compatibility (EMC) is defined as the capability of a device or system to operate satisfactorily in its environment without introducing intolerable electromagnetic disturbances to other equipment ("emissions") and at the same time withstand interferences from the same environment or from an external agent ("immunity" or "susceptibility").

These aspects are crucial in various applications, one of them being aeronautics. An error caused by an external interference in an aircraft or any aerospace vehicle can be fatal, so it is typical to submit any apparatus oriented to this industry to elevated immunity test levels and very restrictive emission limits.

One of the crucial points within EMC is the study of current flux in the metallic structures that enclose the devices. In the case of an aircraft, we are talking about the fuselage, which is the reference voltage for all the electric and electronic aircraft embedded systems. Any currents flowing through the fuselage can perturb critical equipment and induce them to failure if they are not well protected. Studying such currents is mandatory as it can allow to make improvements in the design of aeronautical devices. Further, it can help to discern between interference currents coupled to the useful signals of the devices if the perturbed currents are monitored in real time. Mainly, these currents can be produced by two phenomena:

- HIRF (High Immunity Radiated Fields). They are electromagnetic fields that are produced by high energy systems usually located on land or embarked in another aircraft. Induced electric field levels can be extremely high and affect any type of electronics and digital systems of the aircraft.
- Lightning strikes. A very common phenomenon that can severely affect an aircraft. The impact can be direct, if it falls right on the fuselage of an aircraft, or indirect, if it falls on a nearby location and harmful currents and voltages are induced in the electrical systems due to electromagnetic coupling [1]. This is the effect on which we will focus this work.

The main objective of this work is the construction and validation of a current probe capable of monitoring currents produced by a direct lightning strike[1] on an aircraft. These probes will be placed in the mechanical joints, usually rivets, that attach different fuselage

[1]The overvoltage caused by a direct lightning strike is commonly referred as surge. In this work, this term will be used mainly when referring to currents or voltages produced by a lightning strike.

plates together and must be able to measure hundreds of thousands of amperes, typical current produced by a lightning strike [2]. Note that the study of lightning currents is a challenging task due to the complex shape, materials, joints and apertures found in most aircraft fuselages [3].

This work is part of the coordinated project "eSAFE UAV: Electromagnetic Environmental Effects (E3) on Smart Fuselage and Novel Assembly Technologies in Unmanned Aerial Vehicles (UAV)" of the Ministry of Science, Innovation and Universities of the Government of Spain. The project is executed by the Electromagnetic Compatibility Group (GCEM) of the *Universitat Politècnica de Catalunya* (UPC), the *Instituto Nacional de Técnica Aeroespacial* (INTA) and the *Universidad de Granada* (UGR). This work is the task "O1. To measure the complex current waveforms flowing through screw and rivets that are part of the fuselage assembling" from the subproject "Electromagnetic Interference measurements methods in Smart-Fuselage Unmanned Aerial Vehicles".

1.2 Requirements and specifications

The current probe to be designed must fulfill different features:

- Have sufficient sensitivity to detect currents of at least 50 A.
- Avoid signal clipping at high current flow (200 kA).
- Measure in the bandwidth range of the lightning strike signal. To avoid loss of spectral content, cover severe times the bandwidth. An operating range of 10 kHz - 10 MHz is established.
- Do not use any active components that require an external power supply. Use only passive components.
- Be embedded in a PCB in order to be placed between two fuselage boards.
- Reduced size in order to allow different current probes to be placed in consecutive mechanical joints (rivets).
- Permit to insert a rivet or screw through the probe. The current to be measured should be the one flowing through this joint.

After a brief review of the state of the art of the most commonly used current probes, it is decided that the ideal candidate are the Rogowski Coils [4, 5, 6, 7]. Such probes can be used to measure pulsed currents or high amplitude AC currents. An in-depth study of Rogowski Coils is presented in section 3.

In order to validate the designed current probes, it is necessary to build an appropriate "environment" where tests can be conducted in a repetitive way and minimizing the uncertainty. That is why, as an additional objective, it is proposed the design and validation of a test fixture intended to accommodate the current probes and be able to perform measurements and calibrations of them (section 2). In addition, by using the fixture, the frequency response of the current probe will be determined in

order to correct the signal output and provide a signal identical to the one that flows through the mechanical joints (section 3). Finally, the probe will be validated by simulation and experimentally applying a pulse signal that replicates a lightning strike (section 4).

1.3 Work plan

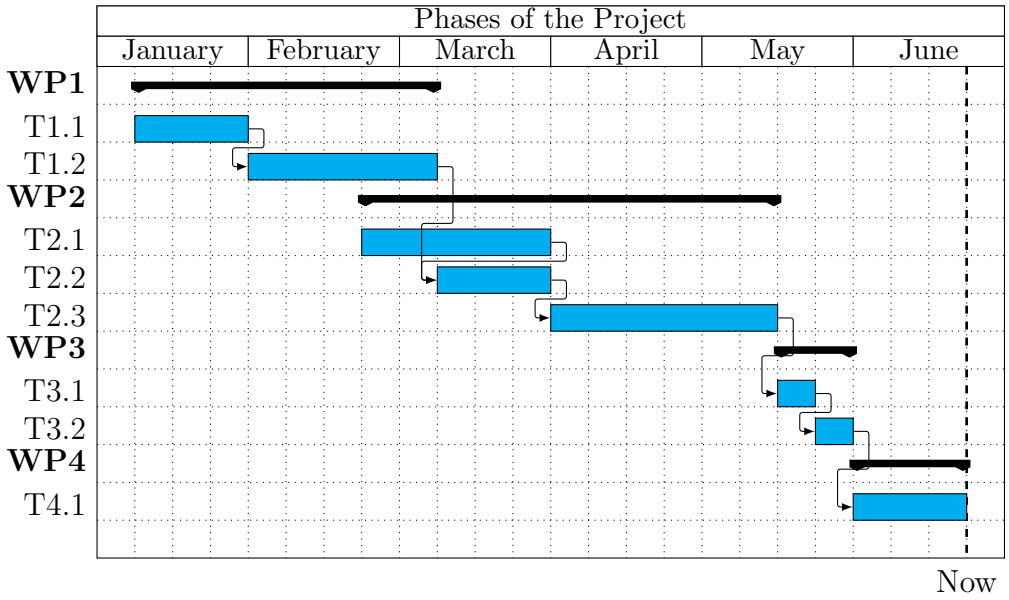

Figure 1: Gantt diagram of the project

- **WP1**: Fixture design and validation.
  - **T1.1**: Simulation with EM FDTD solver.
  - **T1.2**: Experimental characterization.
- **WP2**: Study of Rogowski Coils.
  - **T2.1**: State of the Art research.
  - **T2.2**: Prototype hand-made current probes design and validation.
  - **T2.3**: PCB current probes design and validation.
- **WP3**: Apply to the system application.
  - **T3.1**: Simulation using *LTspice*.
  - **T3.2**: Validation using surge generator.
- **WP4 / T4.1**: Data preparation and memory writing.

There have been no significant incidences in the work plan and it has been executed as defined.

2 Fixture design and validation

2.1 General aspects

When designing current probes, the measuring system that will be used must be taken into account. In particular, how to place the probes as well as the way the current will be injected through them. To make the testing repeatable, a fixture is designed to accommodate up to 5 probes. In this way, the probes remain exactly in the same position to ensure greater reproducibility among various measurements. Besides holding the probes, the fixture also emulates the junction between two fuselage plates of an aircraft. The concept is shown in Figure 2.

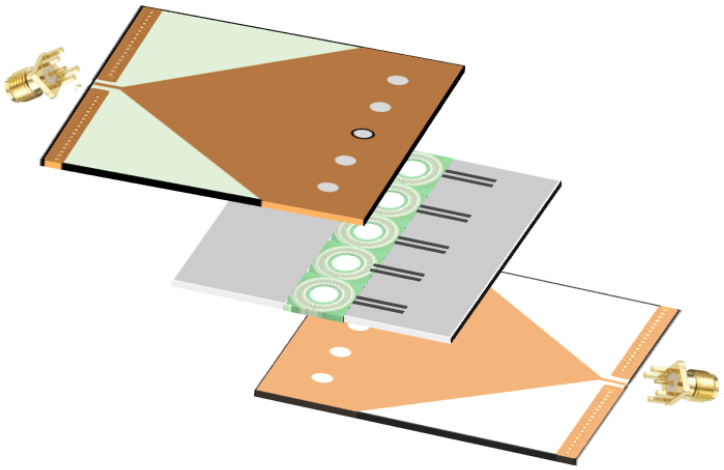

Figure 2: Exploded view of the fixture.

In essence, the fixture is made up of two identical boards. Each board includes an SMA connector and the conductive part progressively extends in a triangular shape until it fills the entire board width. This form is used to avoid possible resonances. At the edge, 5 holes are drilled so that up to 5 mechanical joints can be inserted. An identical board is placed underneath to provide a two-port system in order to be able to investigate different RF parameters, for example scattering parameters. Such parameters will serve to characterize the fixture and validate the frequency ranges in which it is valid. Between the two boards it is possible to add a third PCB dedicated to the current probes which will surround the different mechanical joints, like screws or rivets, that are inserted through the other two boards. Since the fixture itself only acts as a single conductor, it is necessary to provide a proper reference for current returns. For this purpose, two additional parallel boards are added to the fixture, arranged on top and bottom as shown in Figure 3.

In the present section, a numerical model of the fixture is going to be simulated electromagnetically. Subsequently, experimental validation by means of a VNA with the real fixture will be performed. Lastly, a circuital model will be developed to analyze potential discrepancies between simulation and experimental measurements. This last step is found on Appendix A.

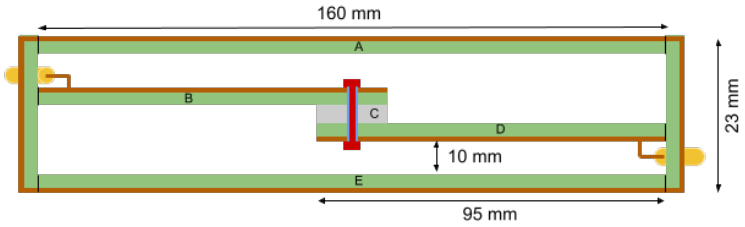

Figure 3: 2D longitudinal view of the fixture.

Furthermore, to facilitate the later study of the results, an additional fixture is designed which consists on a single trace PCB, by overlapping the two identical boards and avoiding mechanical joints, as shown in Figure 4.

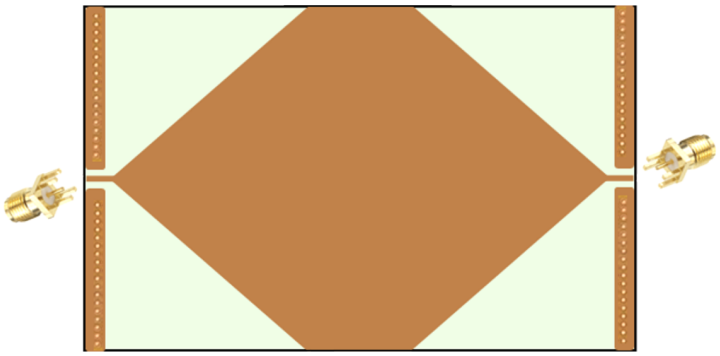

Figure 4: Top view of the continuous PCB trace for the inner line of the test fixture (without junction discontinuities).

Finally, by treating the entire fixture as a TL (transmission line), the single trace PCB might be treated as a way of obtaining the transfer function when no discontinuities (mechanical joints) exist. Obtained results will be useful for more in-depth analysis regarding the effect of adding discontinuities.

2.2 EM simulation

For determining the radiofrequency performance of the text fixture concept model, it is numerically simulated using the Sim4life platform, a full-wave 3D electromagnetic (EM) finite difference time domain (FDTD) simulation software. A CAD model of the two fixtures is built: the complete fixture and the one consisting of a single PCB trace. In the complete fixture, it is possible to include every possible combination of screws to evaluate how the frequency behaviour varies. The single PCB trace fixture, obviously, has a single possible configuration. Both models can be seen in Figure 5. Concerning the used materials, copper elements are treated as PEC (Perfect Electrical Conductors) whereas screws are treated as galvanized iron. Substrates are treated as fibre glass (concretely FR-4). In order to reduce the simulation time (low frequencies imply longer computation time), the scan is performed from 100 MHz to 1 GHz. If we see an ideal response in the low frequency range of the simulation, we can guarantee the same behavior in our operating range (10 kHz - 10 MHz).

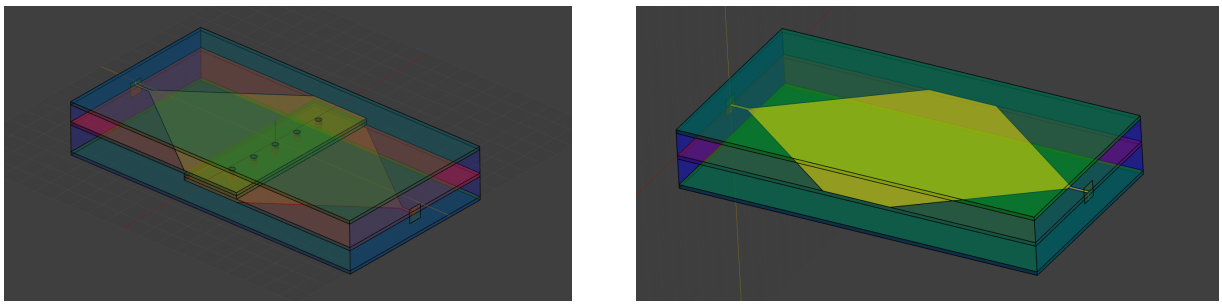

(a) Complete fixture.

(b) Single PCB fixture.

Figure 5: CAD model of the fixture.

Once the model is done, a multi-port simulation is computed for the cases shown in Figure 6. The figure already shows the obtained results. The legend is coded accordingly: “X” for the positions where there is a mechanical joint in place and “0” for the spots without a joint. For example, “00X00” means a configuration where only the central mechanical joint is placed, while “XXXXX” means all screws are used. The combination “00000” means no joints are used. Finally, the trace “Single PCB” corresponds to the fixture formed by a continuous trace.

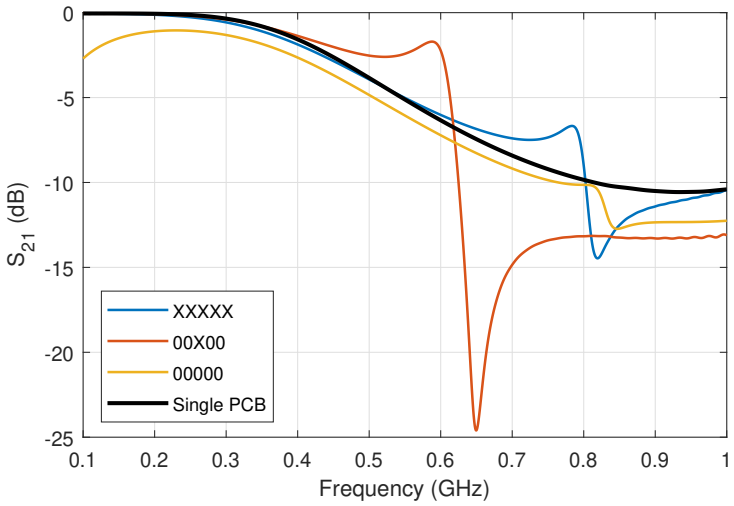

Figure 6: Fixture simulation results.

Regarding the continuous single PCB trace, the frequency response clearly corresponds to a slow roll-off low pass filter. This is coherent with the RC behaviour reasonably expected for this fixture configuration. On the other hand, the "00000" case demonstrates that, as frequency increases, the effect of the capacitive coupling across the overlapped area of the inner line sections is nearly as important as conduction in the 300 MHz – 800 MHz range. However, for the lower part of the frequency range, below 100 MHz, ohmic conduction remains dominant in the continuous single trace PCB.

Furthermore, several numerical simulations have been performed considering different combinations of screws to observe the behaviour thereof (Figure 7).

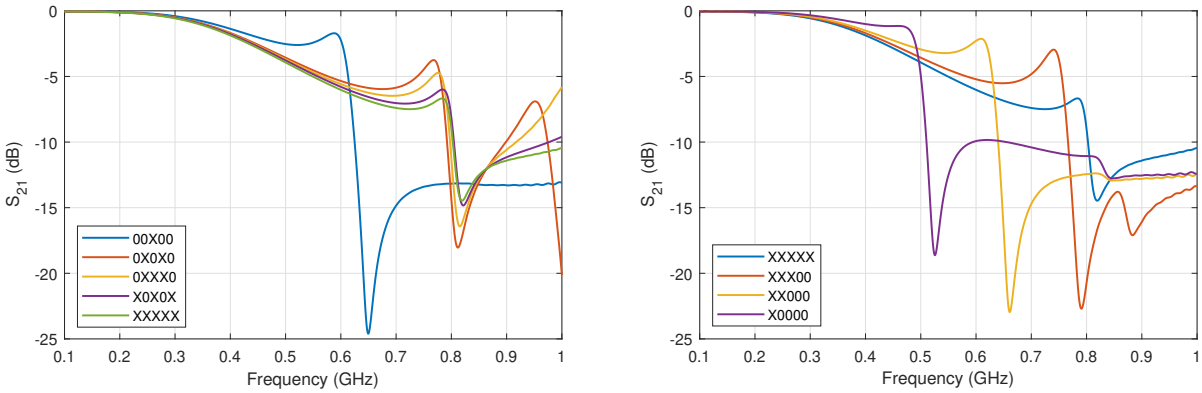

(a) Symmetrical screw combinations.

(b) Asymmetrical screw combinations.

Figure 7: Further simulation results for different combinations of screws.

It is observed how the resonant frequency and the bandwidth change as a function of the number and position used in the different screw configurations of the mechanical joints. All cases behave almost identically up to about 300 MHz – 400 MHz. It is noticeable

that as the number of metal junctions is increased, the S_{21} becomes significantly closer to the behaviour of the single trace PCB, the resonance occurs at a higher frequency and the equivalent total impedance decreases. This phenomenon may be better understood by considering a circuital notion of the fixture, where the two boards are acting as capacitors and the metallic junctions as inductors. When such inductances are combined in parallel, the total inductance decreases leading to a higher resonant frequency. A circuital model of the fixture is found on Appendix A.

2.3 Experimental characterization

Both fixtures are constructed and subsequently experimentally characterised up to 1 GHz. They are constructed with copper as the conductor and FR-4 as the dielectric. SMA connectors were used to terminate the fixture at both ends. Characterisation, in the same way as in the simulation, is carried out by extracting S-parameters of the fixture. On this case, the network analyser (VNA) *Keysight P9374* is employed to obtain the S_{21} parameter. The complete fixture can be seen in the Figure 8a and the measurement set-up in the Figure 8b.

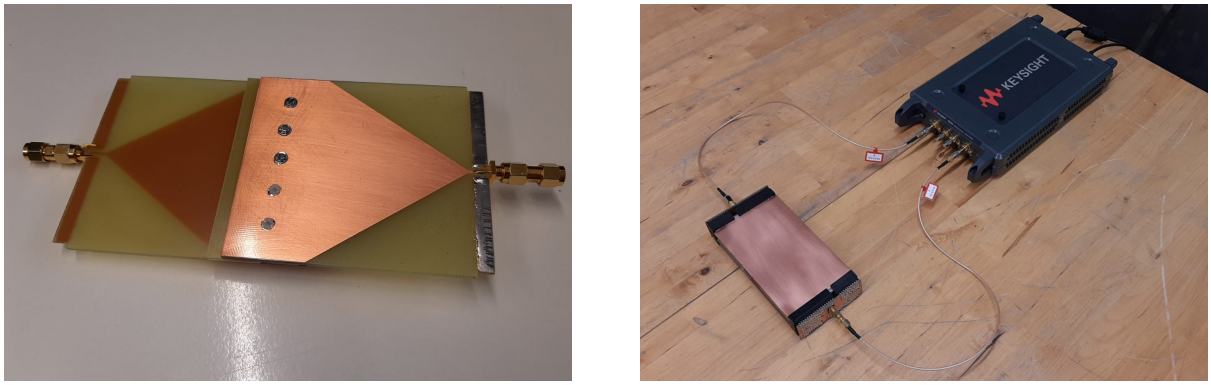

(a) Implemented model. (b) Measurement set-up.

Figure 8: Fixture experimental characterization.

First case examined is the single-trace PCB, which can be treated as the transfer function of the complete fixture without discontinuities (Figure 9). At frequencies below 200 MHz, measurements with VNA and simulations are closely identical, differing by less than 0.2 dB. Beyond that and up to 700 MHz, both responses are very similar. From 700 MHz onwards, discrepancy between them begins to become more significant, as some parameters and parasitic effects not considered during the simulation come into play.

After validating the continous PCB trace, we move on to the complete fixture. In Figure 10, four different configurations are shown. In Figure 10a, it is studied how the fixture behaves capacitively when no metallic junction are present. In Figures 10b, 10c and 10d, the behaviour when screws are present is compared. In general, the fixture offers a good correspondence between the measured and simulated transmission response. Nonetheless, a frequency shift is clearly observed at the first resonance. This frequency shift varies from 30 MHz to 120 MHz depending on the number of junction points used.

It is a future work to model effects causing the frequency shift in order to incorporate them into the simulation so it can be more realistic. By making the simulation as close as possible to reality, time and frequency domain correction factors can be calculated. These will lead to excellent calibration factors.

As a final test, a measurement from 300 kHz to 100 MHz is conducted. It cannot be performed at lower frequencies due to the specifications of the VNA. However, as

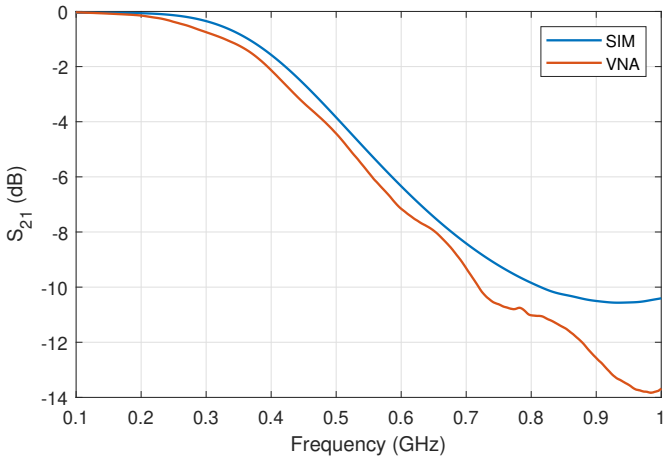

Figure 9: Single PCB trace fixture simulation and VNA comparison.

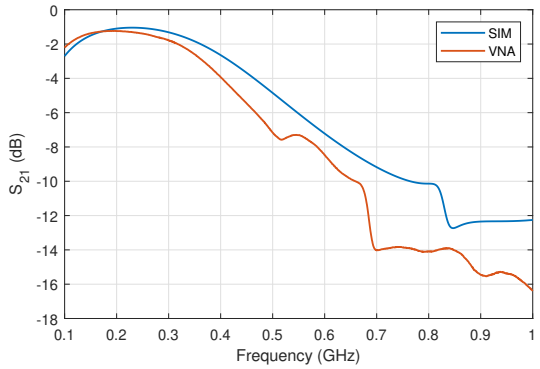

(a) 00000 - No screws.

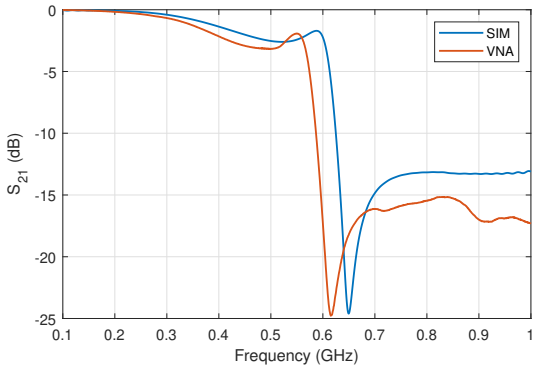

(b) 00X00 - Central screw.

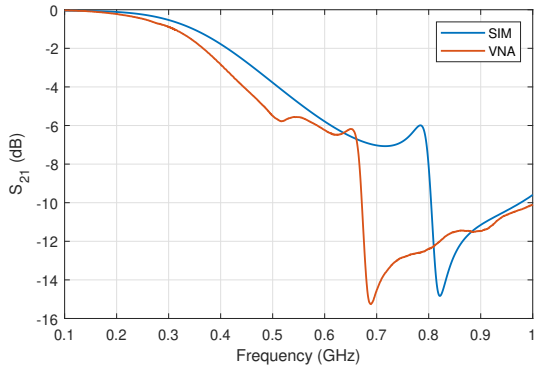

(c) X0X0X - Central and edge screws.

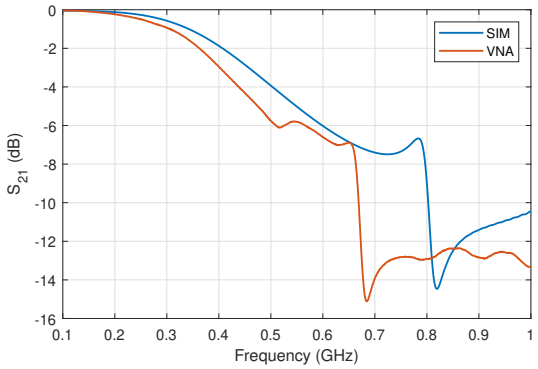

(d) XXXXX - All screws.

Figure 10: Complete fixture comparison of simulation (SIM) results and VNA measurements for 4 different combinations of screws.

the fixture behaves as a simple model with small stray capacitances and inductances, the parasitic effects will only be seen at very high frequencies (as we have seen in the numerical simulation). In other words, attenuation measured at 300 kHz will be virtually identical at 10 kHz. Measure of parameter S_{21} is found on Figure 11. Parameter S_{11} is also measured in this case to check the 50 Ω adaptation of the fixture.

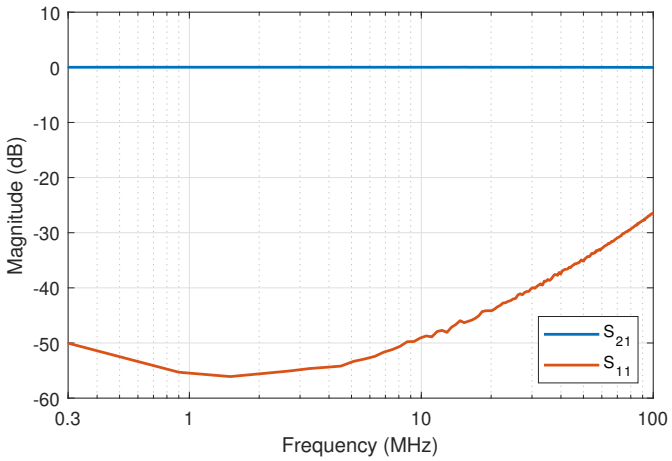

Figure 11: Fixture VNA measurement from 300 kHz to 100 MHz.

As expected, the attenuation is the same than at (100 MHz) and is negligible. The impedance matching is very good up to the working range of the probe (10 MHz). To sum up, since the fixture behaves almost ideally in the frequency range established in this work, no correction factor has to be applied. Merely, when measurements were made with the fixture, results obtained were better than expected, so the study has been continued in order to find the maximum operating range of the fixture. Such information will be useful if it is decided to use the fixture for applications requiring a higher operating frequency, such as HIRF.

3 Study and experimental characterization of Rogowski Coils

3.1 Rogowski coil theory

3.1.1 Rogowski coil basics and modeling

Rogowski coils are a type of non-intrusive isolated sensors used to measure alternating current or high speed pulses. It is basically an air-core helical coil surrounding a conductor from which we want to measure the intensity. The air core allows measuring high amplitude currents (up to mega-amperes) with no saturation. Furthermore, they are easy to use, manufacture and with a small cost, and the output signal can be easily conditioned with passive components [8]. All this features make Rogowski Coils an ideal candidate in order to develop current probes for lightning strike discharges.

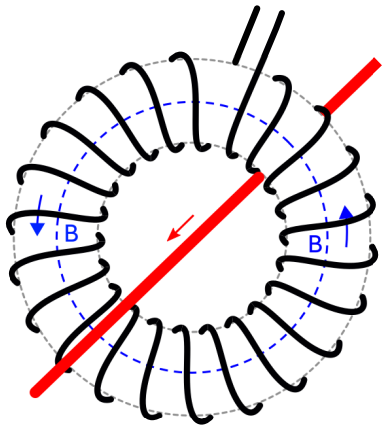

Figure 12: A sample Rogowski Coil.

The output voltage of a Rogowski Coil is proportional to the changing rate of the current. It can be estimated by calculating the magnetic flux circulating though the coil. Assuming rectangular turns, the magnetic flux through a single turn can be calculated using the Ampere's law [9]:

$$\phi(t) = \int B\,dA = \mu_0 h \int_a^b H(x)\,dx = \frac{\mu_0 h}{2\pi} i_1(t) \int_a^b \frac{dx}{x} = \frac{\mu_0 h}{2\pi} \ln(\frac{b}{a}) i_1(t) \tag{1}$$

Therefore, for a general number of turns N, the total differential voltage induced results to:

$$u_d(t) = N\frac{d\phi}{dt} = \frac{\mu_0 N h}{2\pi} \frac{di_1(t)}{dt} \ln\frac{b}{a} = M\frac{di_1(t)}{dt} \tag{2}$$

With M representing the mutual coupling inductance:

$$M = \mu_0 \frac{Nh}{2\pi} \ln \frac{b}{a} \tag{3}$$

Where a is the inner diameter of the coil, b is the total diameter and h the coil height as shown in Figure 13.

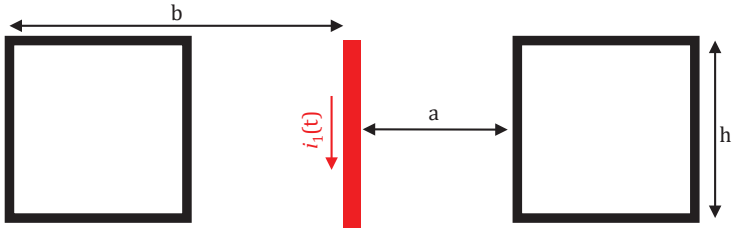

Figure 13: Cross-section of a Rogowski Coil.

Nonetheless, it must be taken into account non-idealities of the Rogowski Coil. Due to the windings, a parasitic series inductance L_s appears as well as a stray capacitance C_p between each turn. Furthermore, the conductive material offers a small series resistance. A simplified model of a Rogowski Coil leads to a 2$^{\text{nd}}$ order RLC circuit:

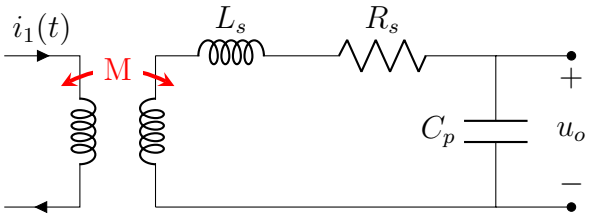

Figure 14: Rogowski Coil RLC model.

Where M is defined in Equation 3 and the other parameters can be calculated as following [10]:

$$L_s = \frac{\mu_0}{2\pi} N^2 h \ln \frac{b}{a} \tag{4}$$

$$C_p = \varepsilon_0 \frac{\pi^2 (a+b)}{\ln \frac{2\sqrt{A/\pi}}{d}} \tag{5}$$

$$R_s = \rho \frac{8N(h+b-a)}{\pi d^2} \tag{6}$$

With $A = h(b-a)/2$ being the area of each turn and d being the diameter of the coil wire. Bear in mind that Equations 1 - 6 assume the core material is air ($\varepsilon_r \simeq 1$ and $\mu_r \simeq 1$).

In order to check the typical Rogowski Coil behaviour, a *LTspice* simulation has been launched. It has been assumed the following values for simulating the probe: $M = 50\,\text{nH}$, $L_s = 1\,\mu\text{H}$, $R_s = 50\,\text{m}\Omega$, $C_p = 10\,\text{pF}$. The relation between the input current and the output voltage is in Figure 15. Note there is a resonance caused by the inductor and the capacitor and the response below the resonance shows a slope of 20 dB/dec.

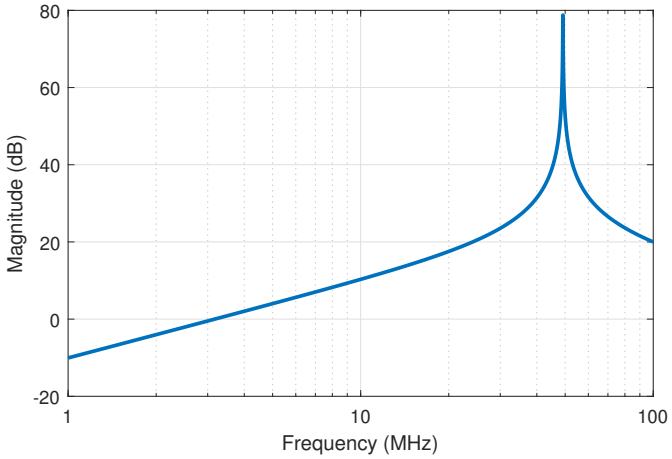

Figure 15: Simulation of Rogowski Coil transfer function.

3.1.2 Analog signal conditioning

The output of the Rogowski Coil requires some signal conditioning in order to be used as a flat-response current probe with no resonances. It consists basically on three stages:

1. *Damping resistance*: A parallel resistor is placed at the output in order to mitigate the self-resonance response of the coil.
2. *Integrator*: Output needs to be integrated in order to make it proportional to the current itself and not to its derivative.
3. *Amplification*: In some cases, sensitivity needs to be increased in order to be able to measure small currents. This is is performed by means of an amplifier that is usually combined with the integrator stage.

We are going to focus on the first two stages. Basically, amplification is not needed in our case because the current to be measured will be in range of kA and the sensitivity with a passive integrator *a priori* will be high enough.

3.1.3 Damping resistor

As the simplified lumped model for the Rogowski Coil is a 2$^{\text{nd}}$ order RLC circuit as stated in Figure 14, the natural response will be self-resonant (Figure 15). The resonance of the coil will provoke a non-flat transfer function, not suitable for the desired application. In order to minimize this effect, a damping resistor R_d is placed in parallel at the output of the coil [11] as shown in the following figure:

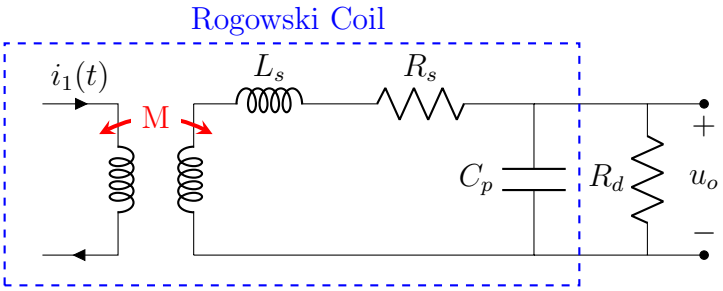

Figure 16: Rogowski Coil schematic with damping resistor.

From the circuit above, the transfer function can be derived [12]:

$$H(s) = \frac{U_0(s)}{I_1(s)} = \frac{Ms}{L_s C_p s^2 + (\frac{L_s}{R_d} + R_s C_p)s + \frac{R_s}{R_d} + 1} \tag{7}$$

From the standard second order transfer function of the form:

$$H(s) = K\frac{\omega_0^2}{s^2 + 2\zeta\omega_0 s + w_0^2} \tag{8}$$

And choosing a value of $\zeta = 1$ in order to make the response critically damped, we can obtain the optimium value for this resistor [13]:

$$R_d = \frac{1}{2\zeta}\sqrt{\frac{L_s}{C_p}} = \frac{1}{\zeta}\pi L_s f_0 \rightarrow R_{d,opt} = \frac{1}{2}\sqrt{\frac{L_s}{C_p}} = \pi L_s f_0 \tag{9}$$

Where $f_0 = \frac{1}{2\pi\sqrt{L_s C_p}}$ is the resonant frequency of the coil.

This effect is shown through a *LTspice* simulation. A current is injected and the output voltage is measured, then, the transfer function is computed. Using Equation 9, the optimum damping resistor for the values previously commented is 158 Ω in order to achieve a critically damped response. In parallel, a simulation has been performed with no damping resistance and also with a resistance lower than the optimal value:

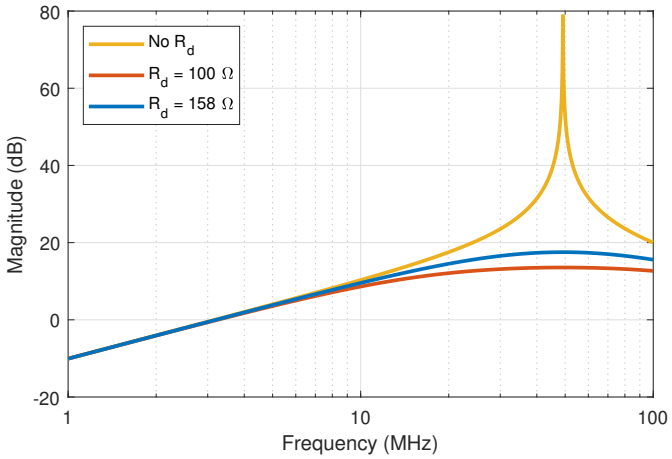

Figure 17: Simulation of Rogowski Coil output with different damping resistors.

Note how the damping resistor eliminates the resonance of the circuit. With the optimum resistance, it is achieved an equilibrium point between reducing the fundamental resonance and maintaining sensitivity at high frequencies. If the resistance is lower than the optimal value, resonance is also suppressed but the overdamped response leads to decrease the sensitivity at high frequencies.

3.1.4 Integrator

As stated in Equation 2, the output voltage induced in the Rogowski Coil is proportional to the derivative of the measured current. Therefore, in order to obtain a plain frequential response the output must be integrated. In order to do so, typically, a RC low-pass filter is used [14, 15]:

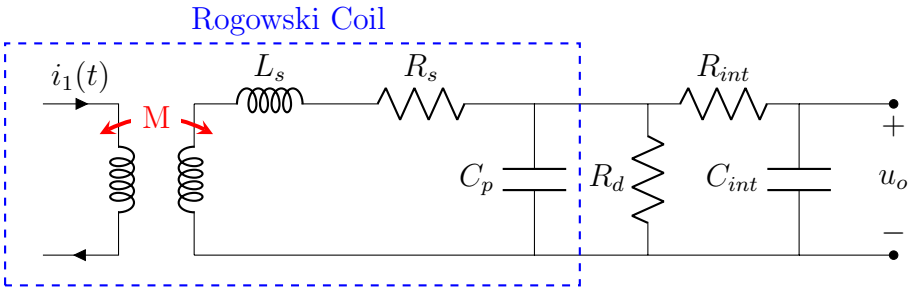

Figure 18: Rogowski Coil schematic with damping resistor and integrator.

Analogously, for frequencies higher than the cut-off frequency, the low-pass filter transfer function decreases 20 dB/dec. As the natural response of the current probe increases 20 dB/dec below the resonance, the resulting slope will be 0 dB/dec between the low-pass filter cut-off frequency and the coil resonant frequency. This will make the probe response between these two points flat, which will determine the operating range of the probe and prevent the acquired signal from being distorted. A simulation with values used in previous section is launched to clarify this concept:

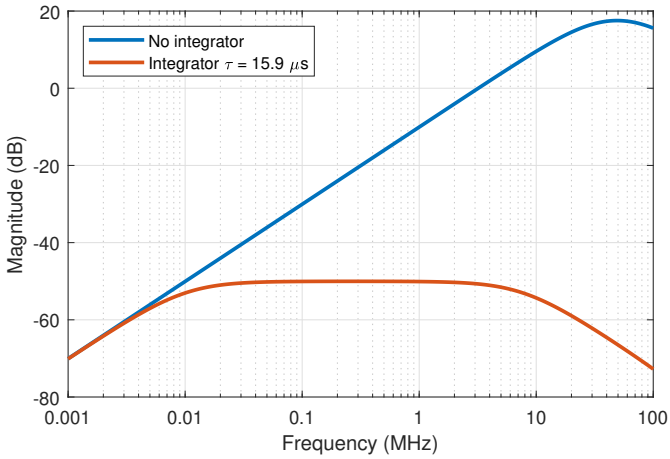

Figure 19: Simulation of Rogowski Coil output with integrator.

The filter used is tuned with a $\tau_{int} = R_{int}C_{int} = 15.9\,\mu s$ ($f_c = 10\,kHz$). It is observed that above the filter cut-off frequency, frequential response gets flat, resulting in a bandwidth from 10 kHz to 7.6 MHz. Nonetheless, since we are employing a passive integrator, the flat response is obtained at the cost of reducing the sensitivity. In many applications where small currents are measured, it is necessary the use of an active integrator employing an op-amp [9], however, this is not required when measuring high currents [14], avoiding a saving in cost, less space on the PCB, and the fact of powering the op-amp with a DC voltage.

3.2 Hand-made current probes

3.2.1 Probes specifications, design and characterization

After studying and analyzing the theoretical behavior of Rogowski Coils, a set of prototype current probes are built with the purpose of validating them experimentally. To do so, enameled copper wire is winded on a nylon washer. The reason for using nylon is that it is a material with a relative magnetic permeability of practically $\mu_r \simeq 1$, which implies that it behaves as air when it comes to magnetic effects. This means that the core will not saturate and linearity at different currents is guaranteed.

It is decided to build three probes with these specifications:

Turns	***d***	***a***	***b***	***h***
N = 20	0.7 mm	8 mm	16 mm	1.5 mm
N = 35	0.7 mm	8 mm	16 mm	1.5 mm
N = 140	0.2 mm	10 mm	20 mm	2 mm

Table 1: Hand-made current probe specifications.

Where d is the wire diameter, a is the internal diameter of the coil, b is the external or total diameter of the coil and h is the coil's height as depicted in Figure 13.

In order to select these parameters, first of all, the number of turns is chosen, and then the diameter of the wire and washer size are adjusted accordingly. The study [16] recommends a ratio between external diameter and internal diameter of the coil a/b from 1.6 to 2.4. In our case, this ratio is set to 2. The built probes can be seen in the following figure:

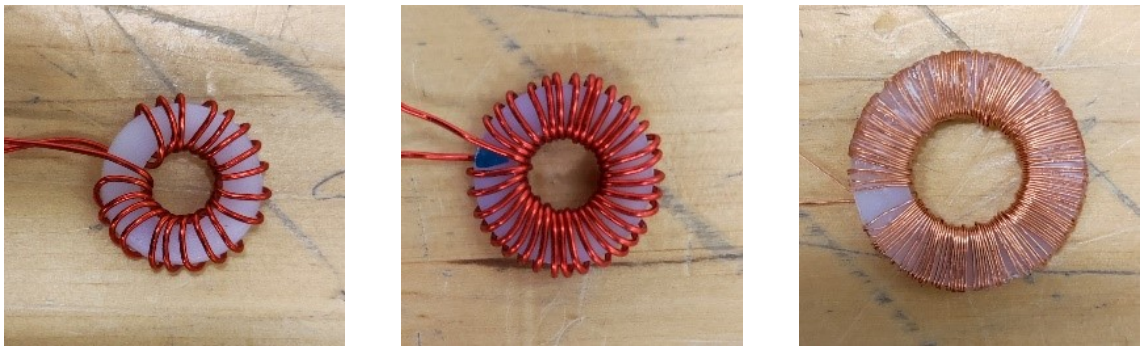

(a) $N = 20$. (b) $N = 35$. (c) $N = 140$.

Figure 20: Hand-made Rogowski Coil based current probes.

Once the probes have been assembled, the parameters of the lumped model can be extracted (remember that the probe behaves as an RLC circuit). First of all, they are calculated theoretically using equations 3 - 6:

Probe	R_s	L_s	C_p	M
N = 20	17 mΩ	83.2 nH	5.5 pF	4.16 nH
N = 35	29.7 mΩ	254.7 nH	5.5 pF	7.28 nH
N = 140	1.83 Ω	5.4 µH	32.7 pF	38.82 nH

Table 2: Theoretically computed RLC parameters for the hand-made current probes.

Subsequently, the corresponding values are obtained experimentally. The first step is to determine the series resistance R_s in DC using a 4-wire multimeter. The 4-wire measurement is necessary since the resistance of the probe is very low and the resistance of the multimeter leads would introduce a significant error.

Then, the impedance of the probe versus frequency is obtained by means of a VNA. In order to obtain this magnitude, Z_{11} parameter is acquired, which already corresponds to the impedance as a function of frequency. Analogously, the equation of the impedance at the output port of the probe is given by:

$$Z(s) = \frac{L_s s + R_s}{L_s C_p s^2 + R_s C_p s + 1} \tag{10}$$

Considering that this is an RLC circuit, the frequential response will present a peak at the resonance frequency with the following value, that will be used later to extract the value of the stray capacitance [16]:

$$\omega_0 = \frac{1}{\sqrt{L_s C_p}} \rightarrow C_p = \frac{1}{L_s {\omega_0}^2} \tag{11}$$

Once the measurement procedure has been defined, the probe is connected to the VNA. VNA model is *Keysight P9374*, capable of measuring from 300 kHz up to 20 GHz. One terminal is connected to GND and the other to the measuring port to determine the Z_{11} parameter. Set-up of the measurement is shown in Figure 21.

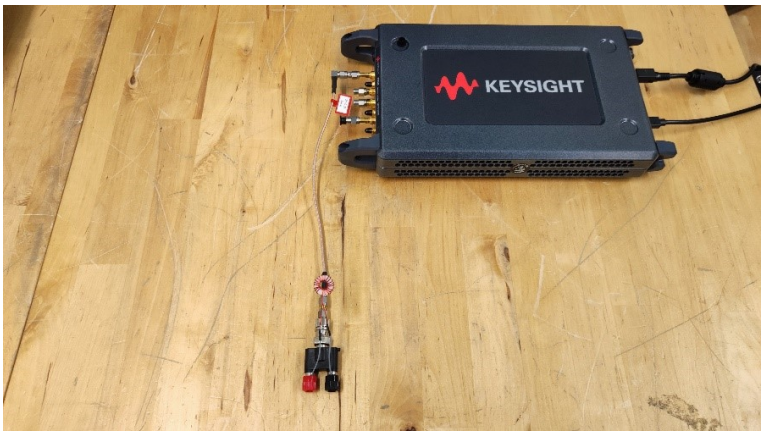

Figure 21: Z_{11} measurement set-up.

After assembling the set-up, measurements of the Z_{11} parameter (magnitude and phase) are performed from 300 kHz to 300 MHz in order to capture the resonance of the circuit. Using the impedance magnitude and the resonance frequency, the model (Equation 10) is adjusted numerically to obtain L_s and C_p. To compute the mutual coupling inductance, and combining Equation 3 and Equation 4, the following relation has been assumed [17]:

$$L_s = N \cdot M \tag{12}$$

Figures 22 - 24 illustrate the experimental measurements as well as the simulation of the model fitted to the values obtained. Parameters are summarized on Table 3.

Probe	$\boldsymbol{R_s}$	$\boldsymbol{L_s}$	$\boldsymbol{C_p}$	$\boldsymbol{M}$
N = 20	29.4 mΩ	315 nH	6.8 pF	15.75 nH
N = 35	56.5 mΩ	560 nH	7.1 pF	16 nH
N = 140	1.36 Ω	8.5 µH	8.1 pF	60.71 nH

Table 3: Measured RLC parameters for the hand-made current probes.

Comparing theoretical values in Table 2 and experimental results obtained by tuning the model in Table 3, it is noticeable that although these values do not match, both are of the same order of magnitude and their validity can be assured. Several reasons cause the results to differ: the coil is not built exactly as the formulas imply; the lengths differ slightly from the values used; the distance between turns is not uniform; parasitic inductances and resistance of the measurement cables used must be taken into account; wire diameter has a certain tolerance and may not coincide with the specifications, etc.

However, the obtained model is really reliable and matches with the measurements made (Figures 22 - 24). Even though there is a small phase error in the low frequency range, this is irrelevant for our application. There is also a small difference in the magnitude of the resonance caused by the coil. In the measurement, quality factor Q of the circuit is much lower due to parasitic capacitances that are not taken into account in the 2$^{\text{nd}}$ order RLC model. Nevertheless, this is not significant as we will not be operating in the frequency range in which the resonance occurs. Consequently, the used circuit model provides a very realistic representation with which the parameters can be accurately extracted.

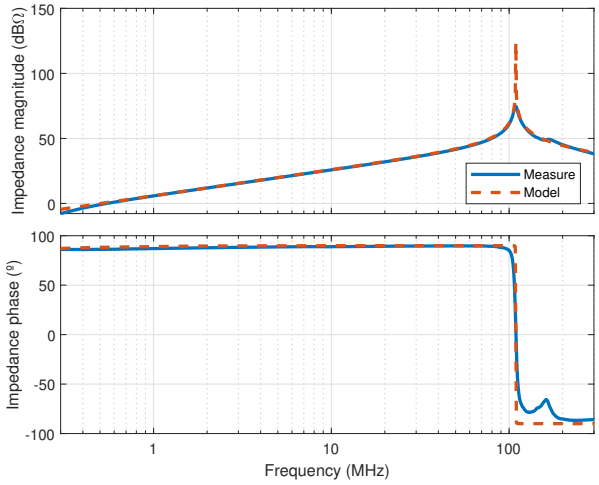

Figure 22: Impedance vs frequency with $N = 20$ turns hand-made probe.

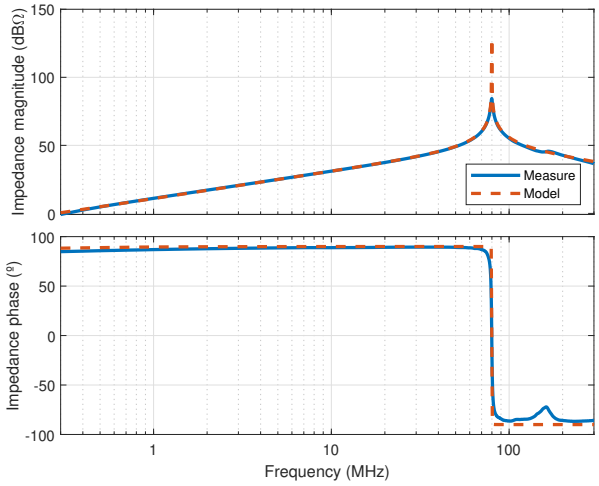

Figure 23: Impedance vs frequency with $N = 35$ turns hand-made probe.

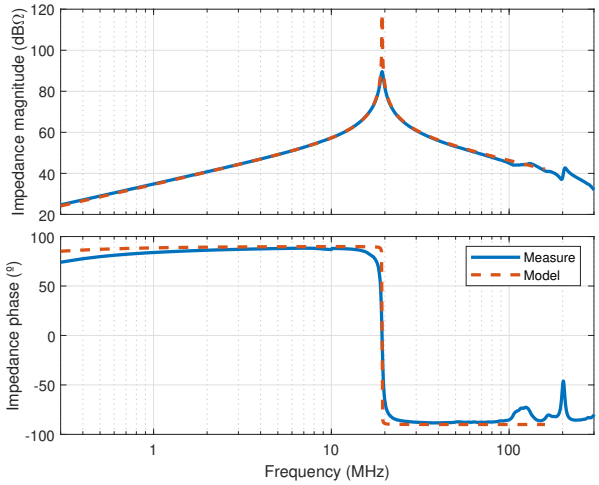

Figure 24: Impedance vs frequency with $N = 140$ turns hand-made probe.

3.2.2 Experimental validation

Validation with an oscilloscope and a function generator

The first experiment for validating the probes consists of injecting a sinusoidal signal into the fixture using a function generator. This signal is injected via one of the connectors of the fixture, while the other is terminated with a T adapter, with one end connected to a 50 Ω load and the other end to the high impedance oscilloscope input. The two hand-made probe leads are connected to a *Tektronix TDP1500* differential voltage probe. The use of a differential probe is required to prevent parasitic capacitances between the hand-made probe and the fixture ground, which may lead to improper measurements [18]. Finally, only one single screw is used within the fixture. Set-up used is shown in Figure 25.

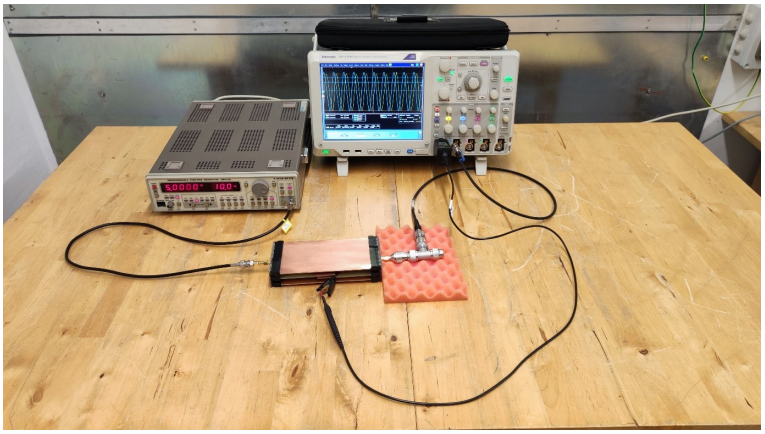

Figure 25: Hand-made probes experimental validation using an oscilloscope and the fixture.

The sweep is performed from 1 MHz to 200 MHz in linear steps of 1 MHz. At each frequency, the RMS voltage value measured on the differential probe is captured (Figure 26).

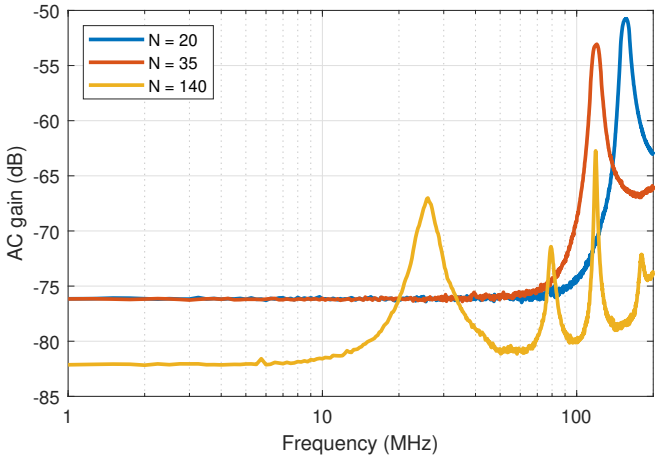

Figure 26: Hand-made probes experimental validation results using an oscilloscope and the fixture.

Different conclusions can be drawn from the previous figure. In first place, if we

have a look at the first resonance produced by the inductance of the coil together with the winding parasitic capacitance, we can notice that the higher the number of turns (and therefore the higher the inductance and capacitance), the lower the frequency of the first resonance, which is consistent with the expected results [19]. Although these measurements provide very interesting information and allow to validate the behavior of the probes at high frequencies, we cannot use this data to calibrate the probes or to observe the behavior at lower frequencies. Note that the flat line that appears below the resonances is not the probe response, but the noise floor due to the low sensitivity of the oscilloscope (In the case of $N = 20$ and $N = 35$ is different from $N = 140$ since a different voltage level was applied).

Despite these results, an identical experiment is conducted, but instead of using the fixture designed, a cable is inserted through the probe. This wire is terminated in a $50\,\Omega$ resistor. The GND of the function generator and the load are connected by a wire mesh to ensure a good conductivity at high frequency (Figure 27). By this experiment we validate whether the effect of the parasitic capacitance to the fixture is influential at frequencies close to resonance. Nonetheless, results obtained using this method and using the fixture are nearly identical and on a functional level do not show any significant difference.

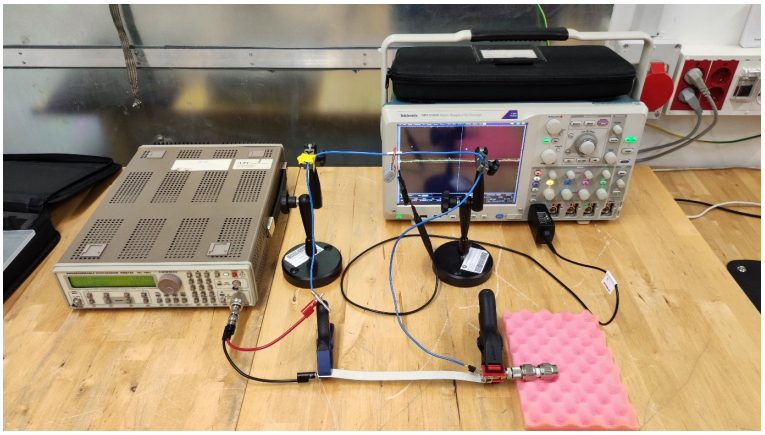

Figure 27: Hand-made probes experimental validation using an oscilloscope and a single cable fixture.

That said, the fixture will be used to validate the probes. Next, the experiments will be repeated with a Vector Network Analyzer in order to evaluate the probes over a wider frequency range and with much higher sensitivity.

Validation with a Vector Network Analyzer

The experiment is repeated using the VNA and the fixture. Port 1 of the VNA is connected to the fixture and Port 2 is connected to one probe lead. The other lead is connected to the GND of Port 2 since the differential probe employed before is only supported by the oscilloscope and cannot be used. The fixture is terminated with a $50\,\Omega$ load. Set-up is shown in Figure 28.

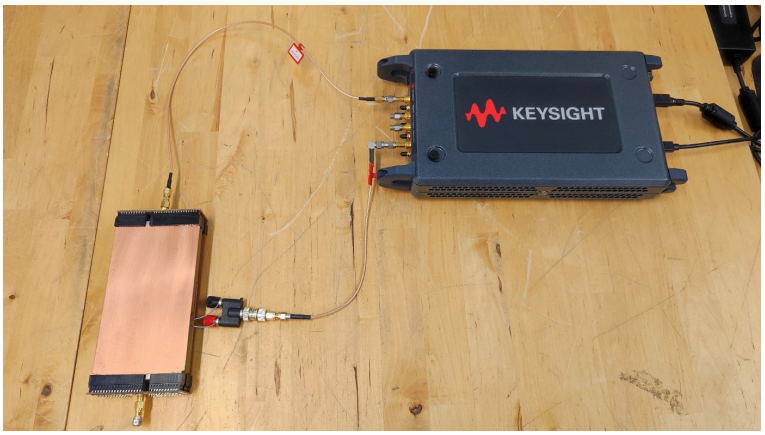

Figure 28: Hand-made probes experimental validation set-up using an VNA.

S_{21} parameter is measured for the different probes. With this parameter it is possible to determine the ratio between the current flowing through the fixture and the output of the probe (in a matched system).

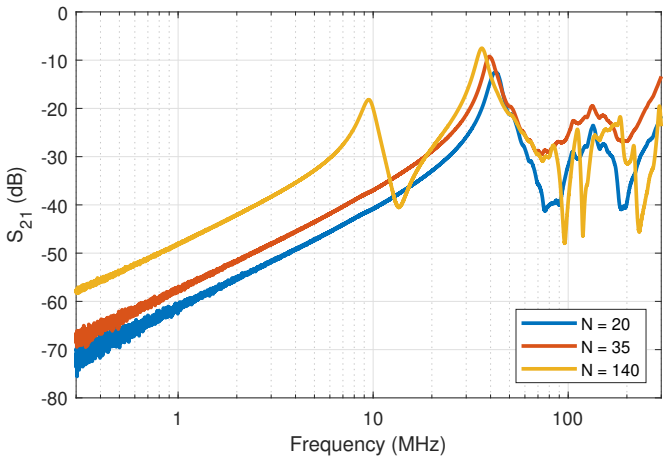

Figure 29: Hand-made probes experimental validation using an VNA.

Observing the results in Figure 29, a notable difference can be seen with the results obtained in the previous experiment (Figure 26). First of all, the resonance frequency do not coincide in both experiments. A reason for this discrepancy is the variability of the parasitic capacitances which influence the testing methods. The input capacitance of the VNA is indeed not the same as the differential probe of the oscilloscope, cables used are different, and in the case of the VNA measurement, we are short circuiting a lead of the probe with the GND of the fixture, so the capacitance also changes.

Another discrepancy lies in the shape of the acquired signal. Whereas with the oscilloscope the only information we could take profit of was the resonance frequency because of the low sensitivity of the oscilloscope, in this experiment we clearly observe the expected shape of the probe (a 20 dB/dec slope below the resonance). The part

above the resonance frequency will not be examined as it does not suit the provided model and will not be of any practical use in our application.

As expected, the higher the number of windings, the higher the sensitivity (it grows logarithmically with the number of turns N), resulting in a trade-off with decreasing the resonance frequency. As it is always necessary to work below the resonance, the usable bandwidth is reduced.

Given the good results achieved, another experiment is performed: replace the metallic screw of the fixture by a Nylon isolated screw, avoiding the ohmic conduction and only allowing the capacitive coupling. It is identical to the case with no screws, however, to keep the fixture structure it is necessary to place at least one. The experiment is carried out with all the probes although only the case for $N = 35$ is presented:

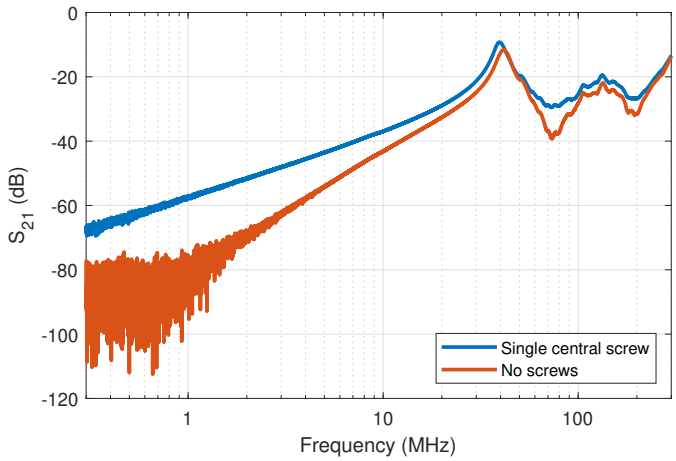

Figure 30: Hand-made probe ($N = 35$) experimental validation using an VNA. Comparison with one single screw and no screws.

With this experiment it is possible to check how adjacent current will couple capacitively to our probe providing invalid data, since it does not correspond to the current flowing through the probe. Ergo, the larger the margin between both measurements, the better. If we set our highest desired working frequency to, for example, 10 MHz, there is an acceptable margin of 6 dB (This value is established as a minimum measure margin by many EMC emission test standards [20]).

Although the margin is enough for the desired application, it can be improved by preventing one of the probe leads from being grounded to GND. A solution might consist of employing an active differential probe, just as we did in the oscilloscope experiment. Nevertheless, these probes usually require an external power supply, which is not available. Alternatively, a balun (balanced-unbalanced lines transformer or balancing unit) can be used (in-depth analysis in Appendix C). Briefly, we switch from a balanced signal to an unbalanced signal and vice versa, while galvanic isolation is provided. In this way, at one side we connect the current probe, which provides a differential voltage, and at the other

we obtain a single-ended signal that we will measure with the VNA. Thus we avoid extra parasitic capacitances to GND, which will eventually decrease the high-frequency margin of our probe.

Figure 31 illustrates the results of the previous case (blue and orange) along with the same measurement but using a balun (yellow and purple):

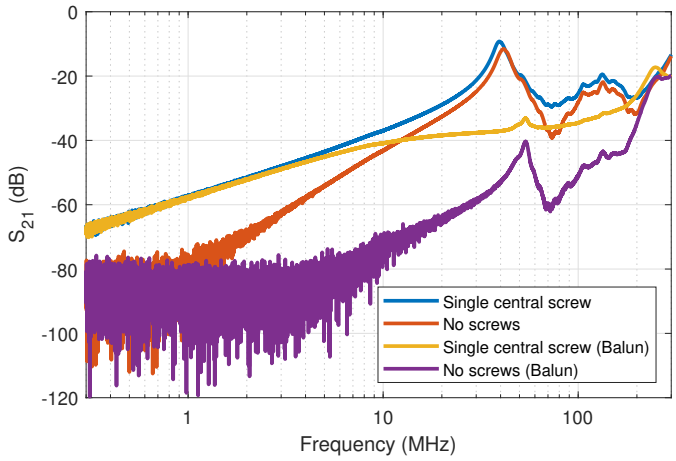

Figure 31: Hand-made probe ($N = 35$) experimental validation using an VNA. Comparison in different cases.

From the illustrated results, we can extract three key factors directly:

- By comparing the blue and yellow line, one can see that adding a balun does not affect the low-frequency part ($< 3\,\text{MHz}$). At higher frequencies, the resonance disappears and the response is flattened. The reason for this is that an extra inductance is added to the probe, which offers a certain impedance at such frequencies. The impedance behaves as a damping resistor, which flattens the resonance. These results validate the feasibility of using a balun for our application, since the signal integrity is not affected in the desired range.
- If we compare the orange and purple line, it can be appreciated that the ratio of the signal respect to the parasitic signal coupled capacitively increases hugely. For example, at 10 MHz it rises from 6 dB to almost 30 dB. Clearly, if a good margin is desired at high frequencies, a balun must be used.
- Comparing again the orange and purple line, it can be seen that they do not decrease below $-80\,\text{dB}$. It is due to the fact that the maximum sensitivity of the VNA is reached and the measured signal is below this level (noise floor). In future cases, if it is necessary to decrease the noise, a preamplifier should be used.

Discussion

Very good results have been achieved in the measurements performed, which are consistent with the shapes obtained in the simulations of the previous section as well as the literature. It must be pointed out that focus has fallen on the range below the

resonance frequency of the current probes since this is the one we will be using for our application. Furthermore, characterizing a Rogowski Coil above the resonance frequency requires a more sophisticated circuit model and it is not recommended to employ them in that range due to the divergences that may occur in a real case.

As a conclusion of the experiments, it is demonstrated that the second order RLC model works, that a trade-off (number of turns) exists between sensitivity and maximum operating frequency, and finally, that if a good margin in terms of capacitive coupling is desired, a balun should be used, particularly when the measuring equipment and the device to be measured share GND.

That said, the hand-made current probes merely served to validate the good performance of the Rogowski Coil. However, manufacturing them on a large scale and using them in a real application is not feasible due to the cost of time, materials, fabrication and discrepancies that may appear.

3.3 PCB Rogowski Coils

3.3.1 Board layout design

After validating the prototypes of the Rogowski probes and proving that they behave as expected, a model is designed in PCB format (Figure 32). Probe is designed as small as possible, always complying with the manufacturer's capabilities (in this case the manufacturer *JLCPCB*). The probe is framed by a 5 cm x 5 cm square. The red color corresponds to the Front copper layer, the blue to the Bottom copper, and green to the Inner copper layer. Finally, yellow corresponds to the silkscreen layer:

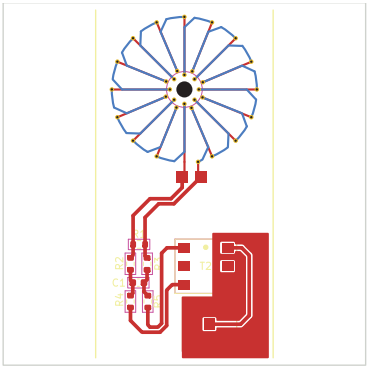

Figure 32: First designed Rogowski Coil in PCB format.

The signal condition stage is described hereafter: there is small GND plane on which a SMA connector can be soldered. The live side of the connector is tied to a small RF transformer[2] (balun) in order to isolate the output signal as mentioned previously. Several footprints are added: 1 capacitor in parallel and 2 resistors in series in order to form an integrator; 1 damping resistor in parallel, and finally 2 resistors in series in order to increase the output impedance. Although none of these solutions may be used, by adding the footprint they can always be implemented quickly and easily. The general layout is shown in Figure 33. Manufactured PCB is presented in Figure 34.

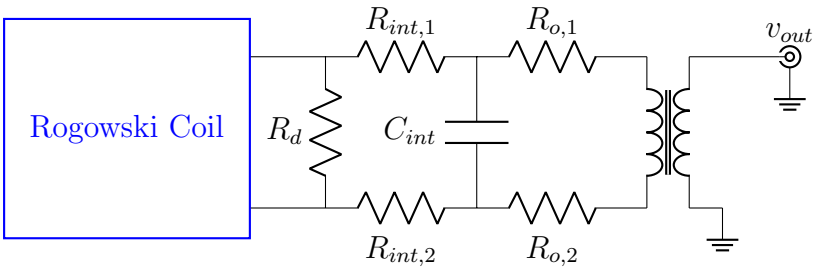

Figure 33: Generic layout of the designed PCB.

[2]RF transformer used is the *Coilcraft PWB2010LB*. This transformer is intended to work in the 3.5 kHz - 125 MHz frequency range. The turn ratio is 1:1 and the maximum current rating is 250 mA.

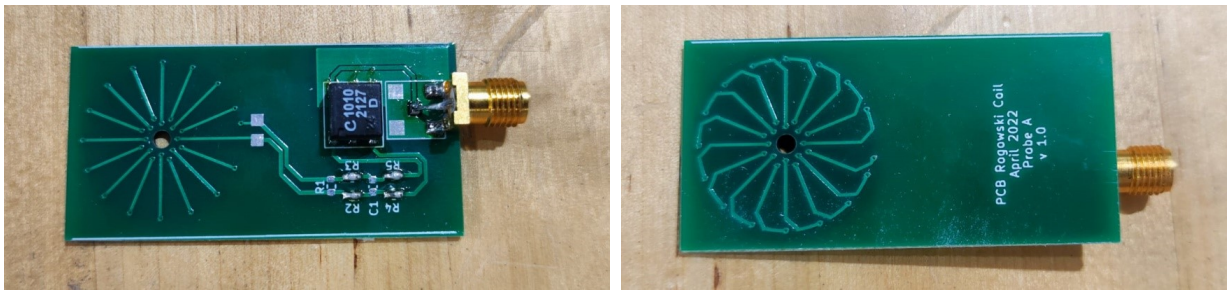

(a) Front layer. (b) Back layer.

Figure 34: Manufactured PCB of a prototype PCB Rogowski Coil.

Once the first prototype of the current probe in PCB format has been designed, which we call it sample A, 5 more models with different features are proposed (Figure 35). The objective is to evaluate all of them and choose the probe with the best behavior.

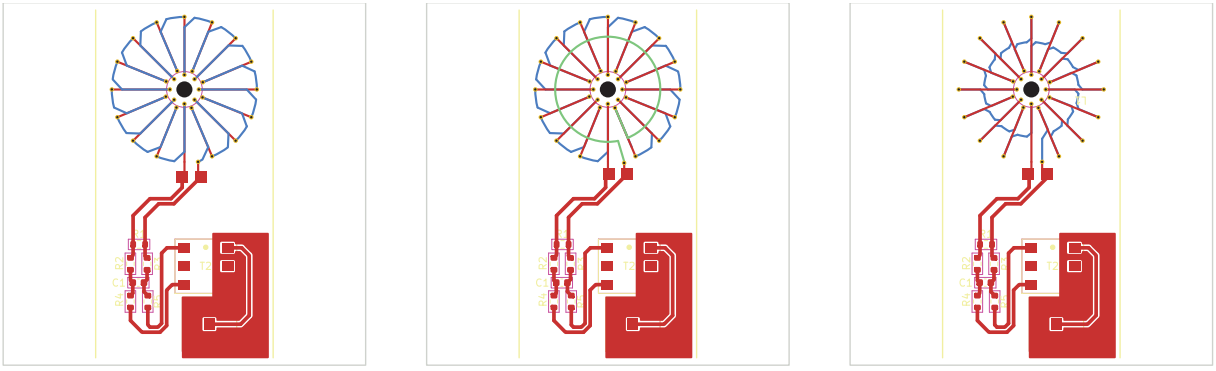

(a) Sample A. (b) Sample B. (c) Sample C.

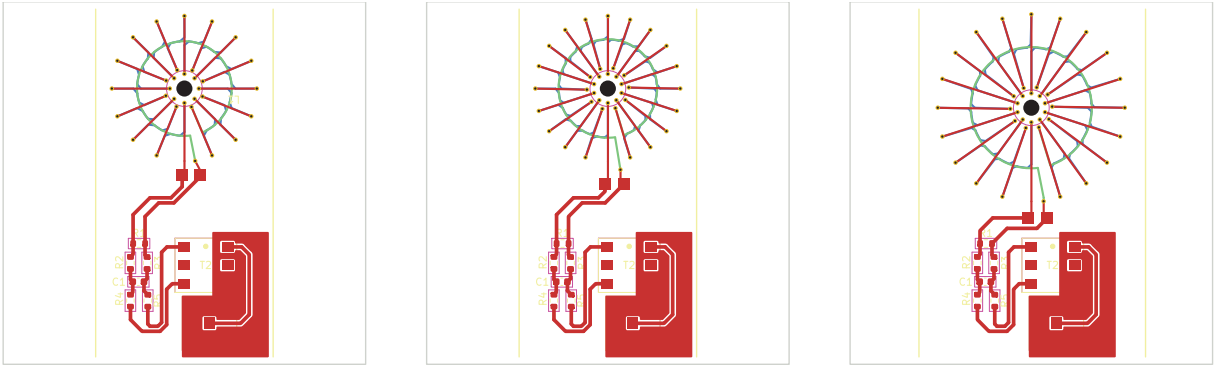

(d) Sample D. (e) Sample E. (f) Sample F.

Figure 35: Layout of the PCB designed current probes.

Signal conditioning stage is identical in all models, however, samples differ in the

number of turns, pattern structure and the use of a return line.

For example, if we compare Sample A and Sample B, we can see that the pattern structure is the same, but sample B includes a return line in the inner copper layer. The return line is added to eliminate the interference to the vertical magnetic field (This effect can be better understood by treating the coil turns as a single line. By adding a return line in the opposite direction, the magnetic field picked up by the signal line is canceled). In this way, we only capture the intended magnetic field in the desired axis [13, 21] . There are other techniques that achieve the same effect, such as differential Rogowski probes [22, 23]. Comparing now sample A and sample C (and their equivalents with return line, Sample B and D respectively) it is shown that although they share the same number of turns, the pattern structure is different. By using different patterns it is possible to increase the mutual inductance and improve the sensitivity [24, 21]. Then, we have sample E, which is equivalent to sample C but with more windings. Finally, sample F would be similar to sample E but with longer turns, having the disadvantage of occupying more space. Sample F is only built in order to check that as larger the size, larger the sensitivity, but it will not be used in our application.

Figure 36 presents the PCBs built with the soldered components and Table 4 summarizes each probe characteristics.

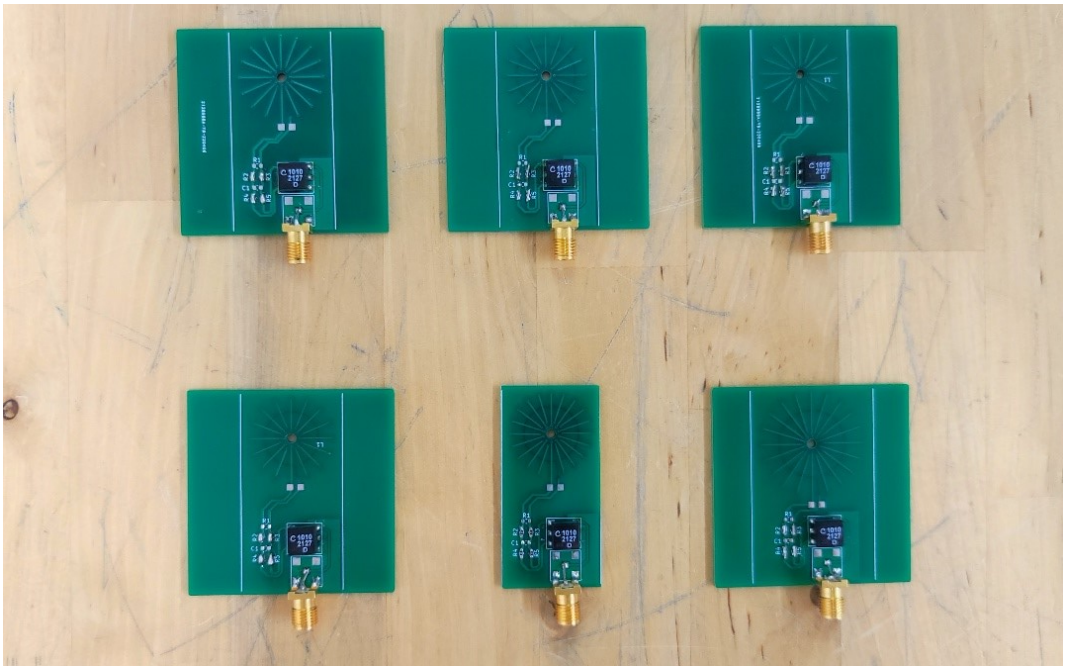

Figure 36: Manufactured PCB Rogowski Coils.

Sample	Pattern structure	N of turns	Return line	Coil radius
A	Standard	16	No	10 mm
B	Standard	16	Yes	10 mm
C	Fishbone	16	No	10 mm
D	Fishbone	16	Yes	10 mm
E	Fishbone	20	Yes	10 mm
F	Fishbone	20	Yes	12.9 mm

Table 4: Manufactured PCB Rogowski Coils characteristics.

3.3.2 Choice of the optimum sample

In this section we will evaluate all the samples experimentally and choose the one which performs better for our desired application. Measurements are performed on the frequency range from 20 kHz to 10 MHz. Higher frequencies are not evaluated now, since the purpose of this measurements is to determine which probe provides the best sensitivity and not to observe its resonant frequency. This experiment is performed using the VNA *Rohde&Schwarz ZVRE* capable of measuring at very low frequencies (from 9 kHz). Port 1 of the analyzer is connected to the fixture. The other end of the fixture is terminated into a 50 Ω load. Port 2 is connected directly to the SMA connector of the PCB current probes. Conditioning signal stage is not used: series resistors are shorted and parallel components are left in open circuit. Set-up is shown in Figure 37 and results are depicted in Figure 38.

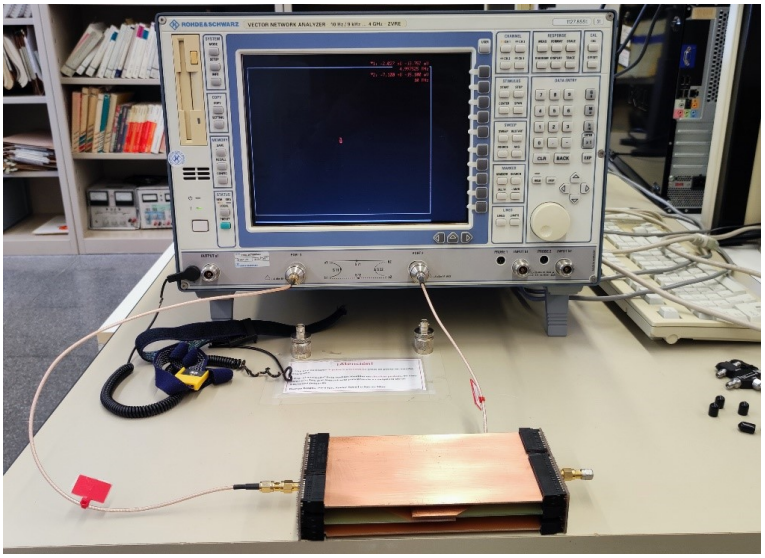

Figure 37: Low-frequency VNA PCB probes measurement set-up.

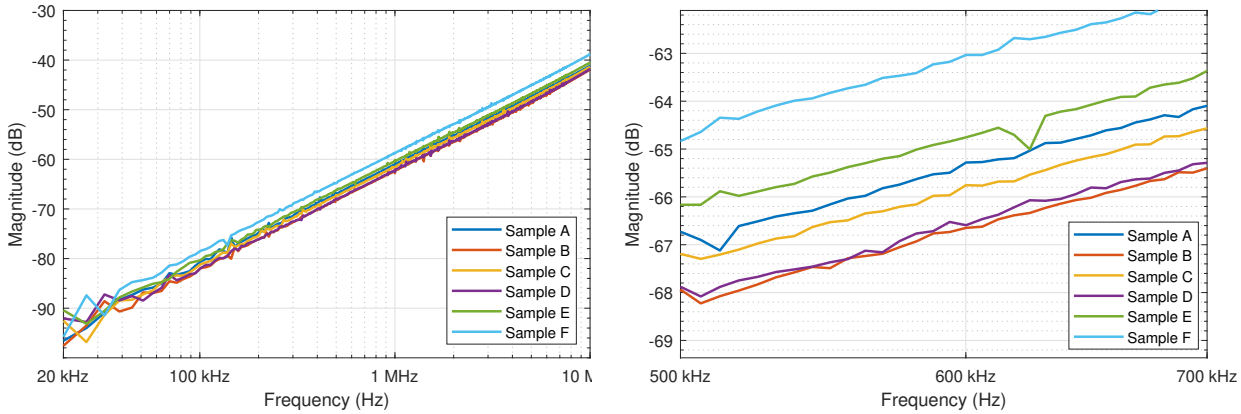

(a) Range from 20 kHz - 10 MHz.

(b) Zoom at 500 kHz - 700 kHz.

Figure 38: Low-frequency VNA characterization of the PCB samples.

To begin with, we can validate that all the probes behave as expected (20 dB/dec slope). Several conclusions can be drawn:

- Comparing Sample A and Sample C (same number of turns, no return line), it can be noticed that the fact of changing the pattern is barely influential, since there is only a difference of 0.2 dB. On the other hand, comparing Samples B and D, which are equal but including a return line, the difference is 0.1 dB.
- If we compare Sample A and Sample B, as well as Sample C and Sample D, we will observe that the addition of the return line has an effect in reducing the sensitivity between 0.5 dB and 0.75 dB. This reduction is due to the increased resistance of the PCB track. Nevertheless, it is advisable to sacrifice this minor sensitivity value and provide immunity to the vertical magnetic field.
- Sample D and Sample E, which both use the same pattern and both have return lines, indicate that increasing the number of turns enhances the sensitivity, as it is expected. Going from 16 turns to 20 turns means an increase in sensitivity of 1.3 dB.
- Finally, examining Sample E and Sample F, which are practically the same but Sample F having longer turns, we obtain an improvement of 1.7 dB.

In conclusion, this confirms what is expected: the higher the number of turns or the larger the size, the higher the sensitivity. According to the previous analysis, **Sample E is chosen as the definitive probe for our application, as it offers the best sensitivity and has a return line**. Sample F is not chosen because, as mentioned above, it is too large and is used only to verify that the larger the size, the higher the sensitivity.

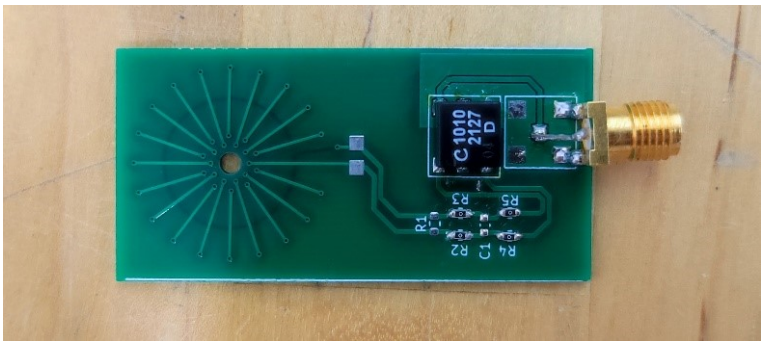

Figure 39: PCB Rogowski Coil - Sample E.

3.3.3 PCB Current probe validation and calibration

Subsequent to the preliminary validation, a calibration of the chosen current probe is performed in order to extract correction factors in the frequency domain. The calibration is carried out from 10 kHz to 100 MHz using two different VNAs: *Rohde&Schwarz ZVRE* for the 10 kHz - 10 MHz frequency range (Set-up in Figure 37) and *Keysight P9374* for the 10 MHz - 100 MHz frequency range (Figure 40).

Calibration is conducted as in most previous experiments: one port of the analyzer is connected to the fixture and the other to the probe. The fixture is terminated at 50 Ω on the other end. Additionally, a 30 dB preamplifier is used on the probe output to obtain better sensitivity during calibration.

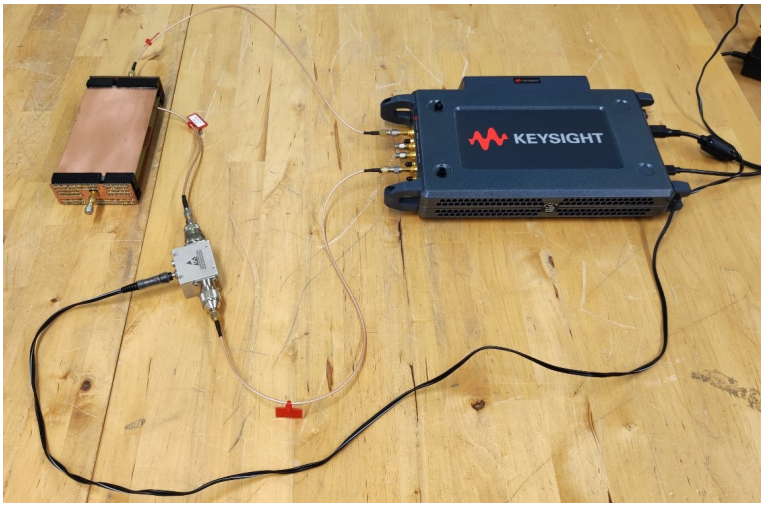

Figure 40: High-frequency VNA PCB probes calibration set-up.

A single metal screw in the center is used to calibrate the probe. Moreover, a measurement is performed keeping the whole set-up but changing only the metallic screw for a Nylon one in order to observe the difference between the capacitive and the magnetic coupling of the probe. Results are shown in the following figure:

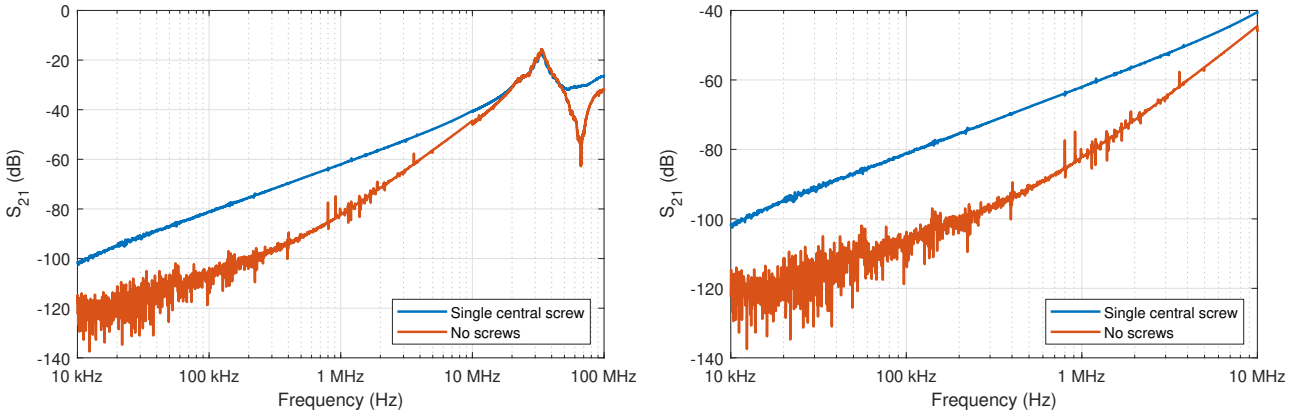

(a) Range from 10 kHz - 100 MHz.

(b) Zoom at 10 kHz - 10 MHz.

Figure 41: VNA calibration of PCB Sample E.

Focusing on the band we are interested in (up to 10 MHz), it is evident that the predicted shape is achieved: an increase of 20 dB/dec below the resonance. Obtaining such results brings great news as it means that with just an integrator we can achieve a flat frequency response and retrieve directly the original signal. Regarding the influence of capacitive coupling, there is 6 dB of margin in the worst case (within our specifications, at 10 MHz), which is an acceptable and adequate margin for our application.

A measurement with an integrator implemented on the PCB itself is performed. Some advantages are that it allows to directly obtain the measured signal at the probe output without having to perform any digital correction. However, by adding the analog integrator, a great amount of sensitivity is lost, as observed in Figure 19. Nonetheless, it might be interesting to run a calibration with an analog integrator to analyze its behavior.

An integrator with time constant $\tau = 18.5\,\mu s$ ($C_{int} = 68\,nF$ and $R_{int} = 100\,\Omega$) is designed. Remind that an integrator can be viewed analogously as a low pass filter (LPF), in this case, with a cut-off frequency of 23.4 kHz. Measures with and without integrator are plotted in Figure 42.

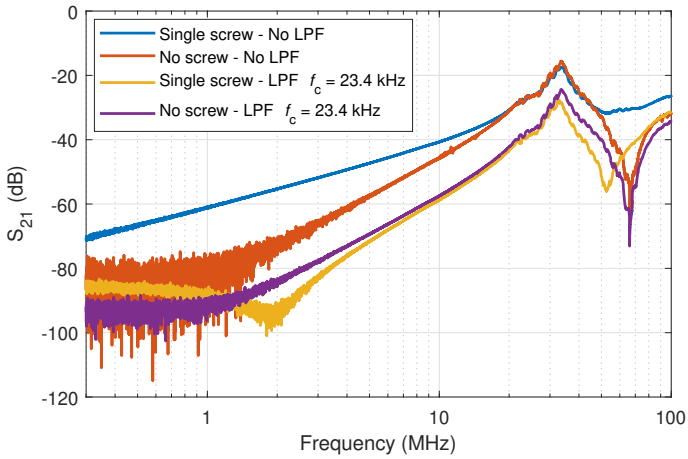

Figure 42: Characterization of Sample E - Comparison with integrator / low-pass filter with $f_c = 23.4\,\text{kHz}$.

The results obtained at the outset can be disconcerting. Theoretically, by adding an integrator, the rising slope is compensated and a completely flat response should be observed. However, it is evident from the yellow line that this is not the case. When performing a measurement with the Nylon screw (purple line), a very similar response is obtained.

After carefully pondering the results and realizing that they do not coincide with the predicted ones, we can draw a clear conclusion. As the sensitivity of the probe is drastically reduced, the frequency response is overlapped by the capacitively coupled noise (orange and purple line), so we can justify not obtaining the expected results. That said, we cannot use an in-circuit analogic integrator due to the fact that the sensitivity obtained is too low to be measureable in our design and under our testing conditions (instruments, fixture, etc.). As the hardware or analogic integrator does not behave as expected, integration will be performed digitally once the signal has been acquired.

Subsequently, an additional test is performed. We are only interested in the spectral content up to 10 MHz, so we modify the values of the previous integrator to form a low pass filter with a cutoff frequency of 15 MHz ($C_{int} = 150\,\text{pF}$ and $R_{int} = 72\,\Omega$). In this way, we filter out all the very high frequency spectral components that are of no interest to us and could result in aliasing in the case of digitally sampling our signal or even clipping the probe output if a very high frequency component with a large magnitude appears. Calibration is repeated and the results are presented in the following figure:

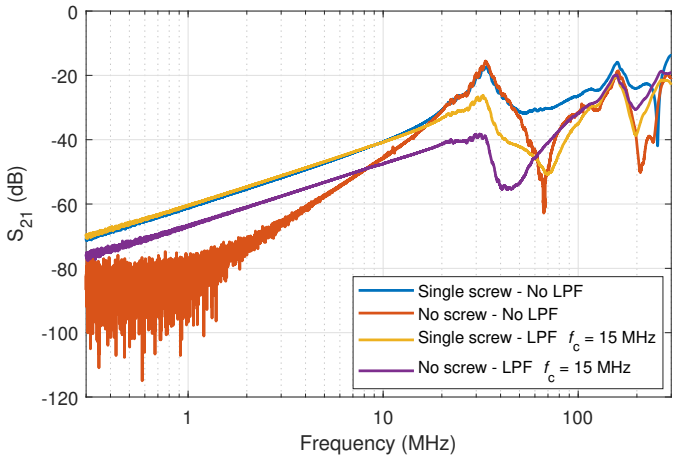

Figure 43: Characterization of Sample E - Comparison with integrator / low-pass filter with $f_c = 15\,\text{MHz}$.

In this case, we see that adding a low pass filter at high frequency does not modify the behavior up to 10 MHz (blue and yellow line). Also we see that the resonance and spectral content up to 100 MHz has been reduced by about 10 dB. Nevertheless, looking at the capacitive coupling (purple line compared to the orange line), it is seen that in the resonance region of the probe it has been reduced by about 20 dB, whereas in the low-frequency region it has been increased. Although these results are interesting, the fact of increasing the noise at low frequency is counterproductive and therefore it is decided to not implement this modification.

Another test performed consists of constructing 3 more identical probes and validating them in the same way. Doing so, repeatability and uncertainty among various replicate probes is examined. Figure 44 displays the calibration results from 300 kHz to 10 MHz. The high frequency part of the usable range of the probe is tested since this is where most divergences can occur. As it is noted, we can clearly appreciate that the three probes have a practically identical response.

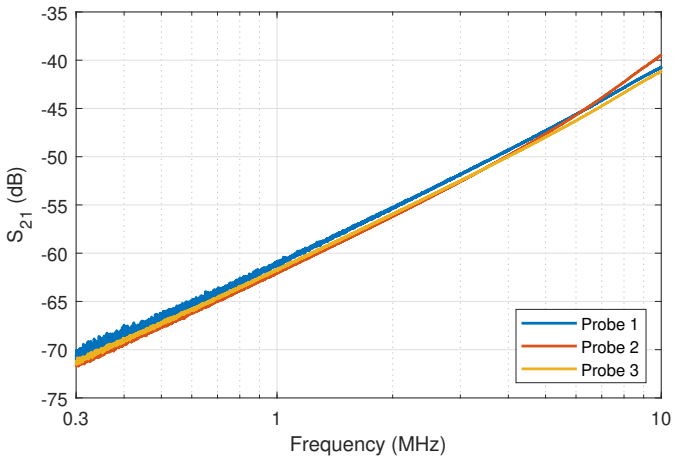

Figure 44: VNA measurement of 3 identical Sample E probes.

Lastly, the last validation performed is the measurement of the capacitive coupling using a metal screw but placing two probes at the edges. In this way we force the ohmic conduction through one of the probes and we can observe the capacitive coupling in the other two (Figure 45). The measurement is performed and the same response as in Figure 41 is achieved (blue line for the central probe with a metallic screw through it and red line for the probes at the ends without screws).

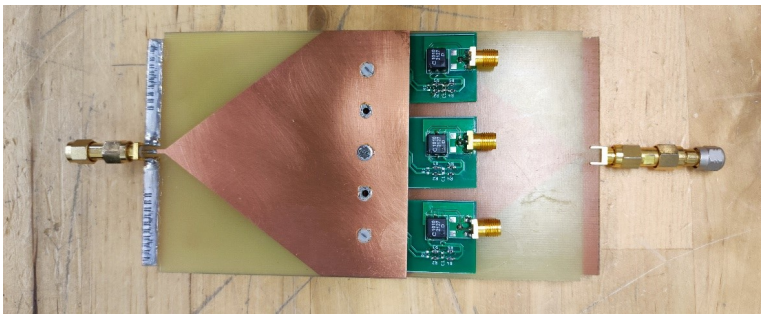

Figure 45: Fixture with 3 PCB current probes.

Probe RLC parameters modelling

The RLC parameters of the probe are calculated for future simulations. The method used is the same as in the previous section, extracting the Z_{11} parameter and fitting the response to a model. However, the model is more complicated now, since an RF transformer is used - which has its own inductance. Remind that the equivalent schematic is shown in Figure 33, where the box labeled "Rogowski Coil" contains the RLC circuit model of a Rogowski Coil (Figure 14).

The impedance in the Laplace domain of such scheme is given in the following equation:

$$Z(s) = \frac{L_T L_s s^2 + L_T R_s s}{L_T L_s C_p s^3 + L_T R_s C_p s^2 + (L_T + L_s)s + R_s} \tag{13}$$

Where L_s is the series inductance of the Rogowski Coil, C_p the parasitic or stray capacitance between windings, R_s the series resistance of the copper and L_T the inductance of the RF transformer. Additionally, the same equation is calculated but assuming a parallel resistance R_p at the output, which will serve to model system losses in the real case (connectors, cables, soldering, inductor/transformer non-idealities, etc.):

$$Z(s) = \frac{L_T L_s s^2 + L_T R_s s}{L_T L_s C_p s^3 + (\frac{L_T L_s}{R_p} + L_T R_s C_p)s^2 + (\frac{R_s L_T}{R_p} + L_T + L_s)s + R_s} \tag{14}$$

Please note that assuming no losses ($R_p \to \infty$), Equation 14 tends to Equation 13.

Find in Figure 46 the experimental measure (continous blue line), the fitted model assuming losses with $R_p = 3.5\,\mathrm{k}\Omega$ (orange dashed line) and the ideal model with no losses

(dotted yellow line). The RF transformer inductance is $L_T = 780\,\mu\text{H}$ (extracted from the component datasheet).

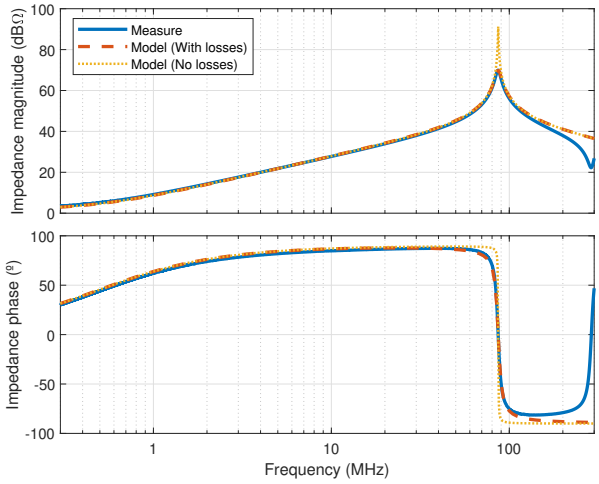

Figure 46: Probe E - Impedance vs frequency.

From the model we can extract the following values, that will be useful in simulating our probe:

- $L_s = 372\,\text{nH}$
- $R_s = 1.2\,\Omega$
- $C_p = 8.7\,\text{pF}$
- $M = 18.5\,\text{nH}$

4 Simulated and experimental validation of the system

In the previous chapter, a probe capable of measuring AC current was built. Its response has been validated as a function of frequency and the circuit parameters have been extracted in order to be able to conduct simulations. In this chapter, we will perform measurements using waveforms targeted to the final application. First, we will run *SPICE* simulations of the current probe and then we will carry out experimental measurements with a surge generator.

4.1 Circuital simulation

The first step to perform the numerical simulation is to mathematically obtain the surge signal. As specified in IEC 61000-4-5[3], such signal can be determined mathematically in order to facilitate simulations. The complete procedure is detailed in Appendix B of this work. The waveform used will be the 8/20 µs waveform (Figure 47), which represents the current flow during a short-circuit [25], that corresponds to the real case of our application. The signal is generated using *MATLAB* and the data is extracted in the time domain.

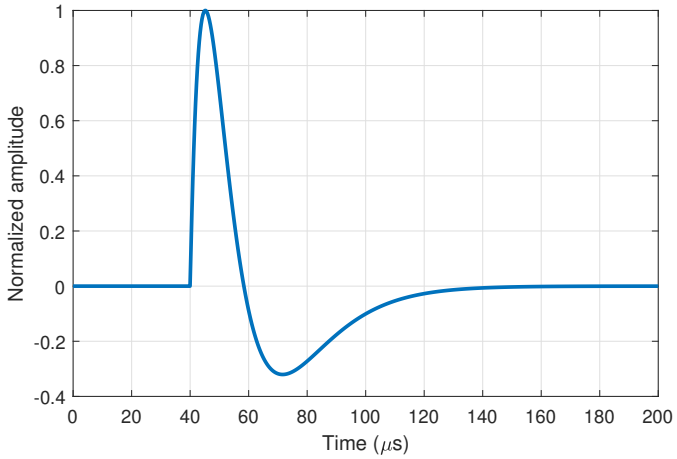

Figure 47: Short-circuit surge current waveform.

LTspice software is used for the circuital simulation. Surge data is added into a current generator with an effective output impedance of 2 Ω. This is the lowest impedance value (implying higher current) offered by a surge generator as defined in [25]. Subsequently, Rogowski's probe circuital model defined in Figure 14 is implemented as well as the RF transformer. The output of the transformer is terminated with a 50 Ω load resistor.

[3]This is the EMC reference standard that addresses immunity requirements, testing techniques and methods, as well as recommended test level ranges to withstand unidirectional surge waves caused by transient overvoltages resulting from lightning strikes and/or switching operations of miscellaneous machinery.

A screenshot of the simulation software can be seen in Figure 48. Note that 1000 MΩ resistors have been added between the floating nodes of the circuit, otherwise the simulator throws a convergence error. Because of the high value of the resistances used, they have absolutely no effect on the simulation results.

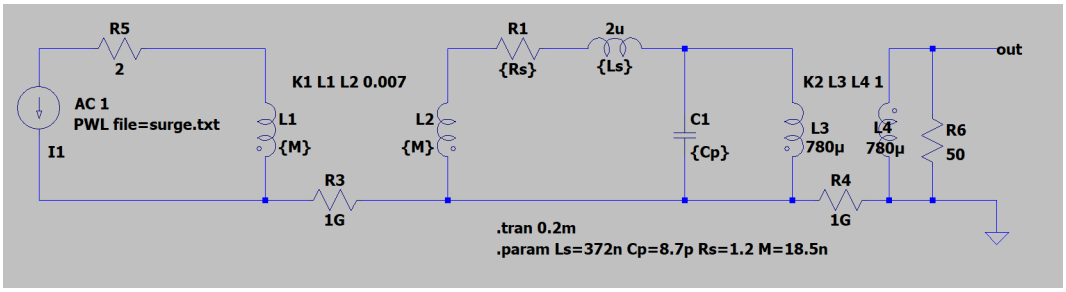

Figure 48: Simulation of the system with *LTspice*.

A transient simulation of the circuit is launched to observe the behavior of the probe when the surge signal is applied. Remember that the probe produces an output signal proportional to the derivative of the input signal:

$$v_{out}(t) = k\frac{\mathrm{d}i_1(t)}{\mathrm{d}t} \tag{15}$$

Where k is a factor that in practice depends on different conditions, such as mutual inductance, system losses, percentage of coupled power, etc.

Integrating the output yields the input waveform multiplied by this factor. When integrating the voltage, a constant is obtained. This is equivalent to a DC voltage offset that in this case is 0, by definition of the surge signal and the impossibility of Rogowski Coils to measure DC signals.

$$\int v_{out}(t)\mathrm{d}t = \int k\frac{\mathrm{d}i_1(t)}{\mathrm{d}t}\mathrm{d}t = k'i_1(t) + V_{DC} \xrightarrow[V_{DC}=0]{} \int v_{out}(t)\mathrm{d}t = k'i_1(t) \tag{16}$$

Figure 49 shows normalized input current (black line), current probe output (blue line), and the integrated probe output (orange dashed line). We can clearly notice how the integrated signal coincides perfectly with the input signal, thus validating that the probe is working properly, at least in the *SPICE* simulation.

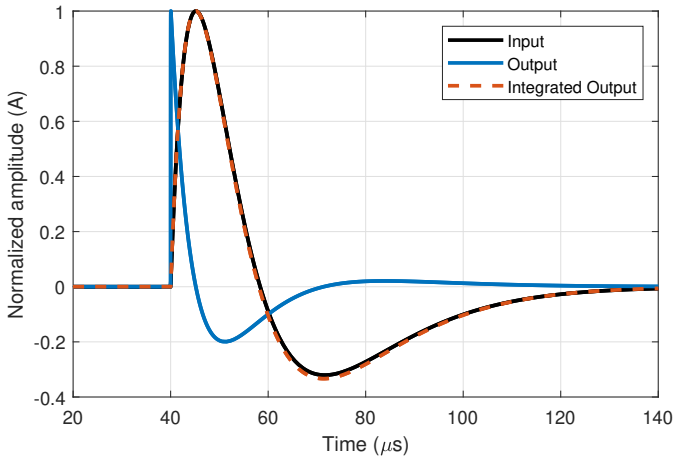

Figure 49: Simulation results with the modeled current probe.

It is important to remark that the model used to emulate the probe in a *SPICE* simulator is valid to obtain the waveform and/or the frequential content of the signal. Nevertheless, it is very difficult to accurately model the fixture and the magnetic coupling from the fixture to the sensor, therefore, in the current/voltage amplitude values, we are considering only the probe in a theoretical way without taking into account details of the real system. Furthermore, the sensitivity obtained in simulation is ideal and will never be overwhelmed by the thermal noise of the measuring instrument. This is a critical point if small amplitude currents are going to be measured.

To summarize, the computational simulation is useful to validate the frequency behavior of the probe, but experimental studies must be conducted in order to verify the sensitivity of the probe.

4.2 Experimental validation

Experimental validation is performed using the surge generator *Teseq NSG 3040* (Figure 50). The generator is capable of delivering output voltages from 200 V up to 4400 V, which, with a minimum output impedance of 2 Ω, translate to currents from 100 A up to 2200 A respectively, ideal for validating our application.

Figure 50: Teseq NSG 3040 Surge generator.

The fixture with a single metal screw is connected to the generator output. A shielded cable is cut and the fixture is placed in the middle. A 10 dB attenuator is attached to the output of our current probe and connected to an oscilloscope with 50 Ω input. Additionally, a calibrated shunt resistor (SDN-414-05) of 50.25 mΩ is also added to the cable. The shunt is connected to a differential high voltage probe in order to measure the current in a accurate manner and compare it with the output of the Rogowski Coil.

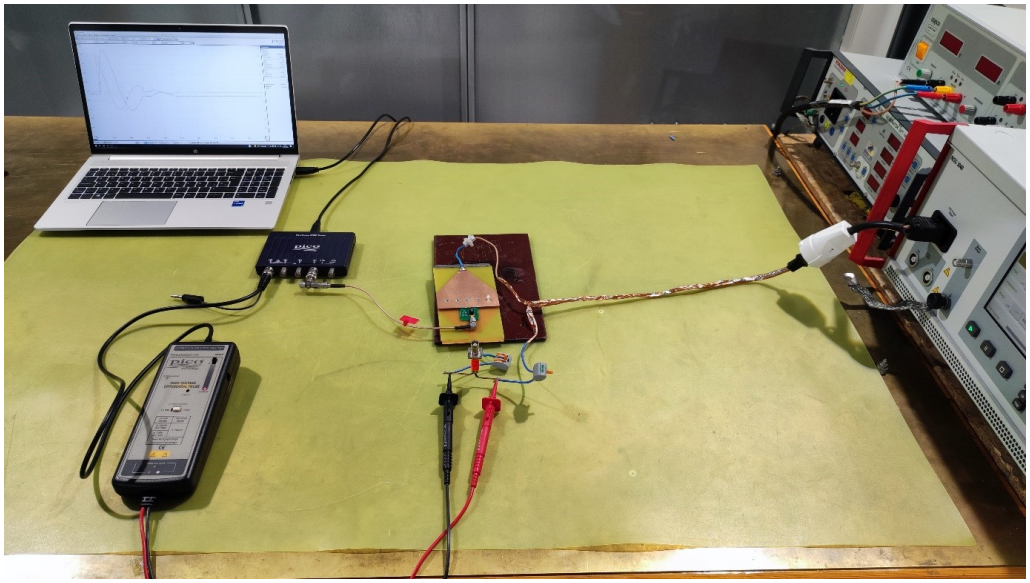

Figure 51: Set-up used for surge validation.

Oscilloscope used is a *Picoscope 2406B* with a bandwidth of 50 MHz, a sampling

rate of 500 MSa/s and an enhanced 12-bit resolution. It is controlled with a laptop and the signal is acquired using MATLAB, which performs a digital integration using the embedded function *cumtrapz()*. This function computes the approximate cumulative integral of a vector via the trapezoidal method with unit spacing [26].

The generator is adjusted to provide a voltage output of 2000 V, equivalent to a current of 1000 A, and then the test is launched. In Figure 52 we can observe the current measured with the shunt (black line), the current probe signal measured by the oscilloscope (blue line) and the same signal integrated digitally (orange dashed line).

The probe output signal has been multiplied by a certain factor so the peak current amplitude matches the shunt resistance measurement. This factor has to be extracted experimentally assuming that the shunt is ideal, since determining it theoretically is very complex due to the losses and non-idealities of all the elements conforming the system (cables, generator, fixture, probe, parasitic elements, etc.). Note that the measured current is slightly lower than the theoretical 1000 A output of the generator. The generator offers an output impedance of 2 Ω, so the resistance of the cables and the fixture itself will cause the equivalent output impedance to increase and therefore the short-circuit current to slightly decrease.

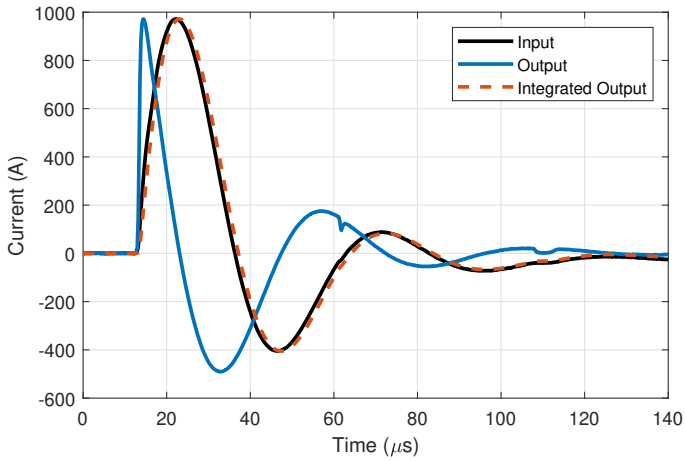

Figure 52: Experimental measurement of a surge current of 1000 A.

As it is seen, the probe works remarkably well, the waveform coincides perfectly with the surge signal and no distortion nor clipping are present. The only noticeable effect that can be mentioned is a short time delay in the measurement of the probe of approximately 830 ns, probably produced by the output cable and the digital integrator. This is a very small and negligible value, which can be easily compensated as it is repeatable and does not have any effect on the shape of the signal itself.

The final test to validate the feasibility of the probe for our application is to check the linearity of the sensitivity of the current probe. Sensitivity indicates how much the output magnitude (voltage or current) changes in relation to the input magnitude (current). In other words, how many volts or amperes we have at the output for each ampere measured

by the probe. This quantity, that is constant, must remain the same or offer very little variability independently of the value of the input magnitude (known as linearity). Bad linearity would lead to signal distortion. A sweep is performed from 500 A to 1500 A and linearity is computed for each case (Figure 53).

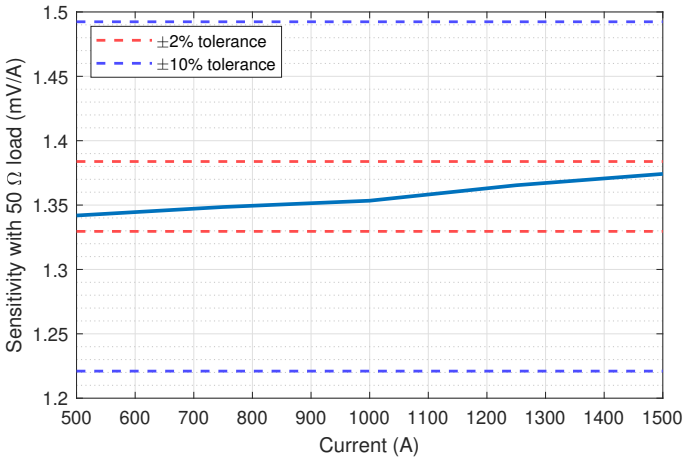

Figure 53: Current probe sensitivity with 50 Ω load.

It can be noted that sensitivity is within a tolerance of ±2% over the measured range. This is a very good value, since the measurement with the surge generator could have as much as ±10% of tolerance [25]. Thus, it can be assured that our probe behaves properly in the time domain (no distortion of the input waveform), and in terms of the linearity of the sensitivity (the output current is always proportional to the input current independently of its value). The probe works successfully and can be easily extrapolated to be placed on the fuselage of an aircraft.

5 Conclusions and future work

5.1 Conclusions

Several conclusions can be drawn from each section of this work. Regarding the fixture designed to evaluate the current probes, results obtained were much better than those expected. For the frequential range defined in this work (10 kHz - 10 MHz), fixture has behaved ideally and no correction factor or calibration was required. Nevertheless, it was decided to evaluate the fixture and simulate it numerically at higher frequencies in order to see up to what point its performance is acceptable. This validation will allow in the future to extrapolate it to other applications that require a higher working frequency such as the evaluation of effects produced by HIRF (High Immunity Radiated Field). In addition, the fixture design was also an opportunity to familiarize with FDTD electromagnetic simulators. Such simulators are very powerful and allow to draw numerous conclusions and outcomes in a wide range of applications.

Concerning the design of the current probes based on Rogowski Coils, initially, a hand-made prototype was built, which consisted of "sewing" enameled copper wire to Nylon washers and then testing its behaviour. There were experiments that did not show significant results, such as measurement with a function generator and an oscilloscope, due to the low power output of the generator as well as the low sensitivity of the oscilloscope. Nevertheless, by using a VNA it was possible to obtain enough sensitivity to characterize the current probes experimentally. Also, it was found that, because of stray capacitances, it was required to add an RF transformer at the output to provide galvanic isolation. In addition, by measuring the impedance of the probe and creating a mathematical model to reproduce the response, circuit parameters could be extracted. This was later useful in order to perform circuit simulations using *LTspice*.

After an extensive study of the state of the art and thanks to the validation of the preliminary probes and the concordance of the prototypes with the theory, it was possible to build prototypes in embedded PCB format. Six prototypes were made and the one with the best characteristics was selected. Also, although it was not used, the option of implementing different signal conditioning techniques such as damping resistance or integrator was provided. First of all, the fact of matching the output to a $50\,\Omega$ system implicitly means the addition of a damping resistor, so there was no need to add an additional resistance. Regarding the built-in integrator, several experiments were conducted with not very convincing results, so it was decided to implement it digitally with the advantage of preserving a good sensitivity. Finally, the mathematical model was adapted to include the RF transformer, a calibration was performed, and then the circuit parameters of the PCB probe were obtained.

Subsequently, it was decided to evaluate the sensors using the surge signal (the overvoltage in case of a direct lightning strike). First of all, the probe was verified to work as expected through circuit simulation using *LTspice*. No signal distortion was observed and the integrated output completely coincides with the input. Afterwards, a surge generator was used to perform the experimental validation. The fixture and a

calibrated shunt resistor were used to measure the current in a "controlled" way and compare the measurements. Using a current of 1000 A, it was observed that the reference measurements and the current probe measurements match properly.

Last step to be performed was to check the linearity of the sensitivity of the probe. Different current levels were tested and a sensitivity of 1.36 V/kA ±2% was determined. It is a very satisfactory value, since the standard that describes the specifications of the surge generator equipment allows up to ±10% of tolerance on the voltage/current magnitude of the generated signal.

Regarding the maximum and minimum range of the sensor, since there is no magnetic saturation of the core, it only depends on the range, accuracy, resolution and noise margin of the measuring instrument used. For the target range (50 A to 200 kA), this results in a output voltage (in a 50 Ω load) of 68 mV to 272 V. Current measured will depend on the number of rivets joining the fuselage plates. For few rivets, a higher current will flow through the probe, so it would be advisable to add an attenuator or even add series resistors on the PCB in order to attenuate the output. For many rivets, current will be lower and output voltage can be measured without any problem by any oscilloscope or A/D converter.

To summarize, the work has been satisfactorily completed and the proposed objectives and work plan have been fulfilled. The current probe manufactured complies with all the established specifications.

5.2 Future work

Several challenges have been stated to be completed in the near future:

- To model circuitally the designed fixture and to improve the electromagnetic simulation to include connectors and different system losses. Even though it has not been necessary in this work, the fixture could be used to validate other higher frequency effects in aircraft, such as HIRF.
- Design a fiber optic link. This is the last assignment of the task proposed by the research project where this thesis is integrated. Instead of using an RF connector, the aim is to use fiber optics in order to avoid external disturbances and distribute the signal over significant distances with practically no attenuation. Moreover, this is a very interesting aspect, since there is literature research about placing optical fibers inside the fuselage panels. However, it should be verified whether the current generated by the lightning strike surge is sufficient to polarize the LEDs/lasers used to transmit optically.
- To calibrate the measuring system in real, in-operando, conditions and to correct from the measurements the effect of embedding the sensor into the fuselage. This item would be carried out in collaboration with the other research project partners.
- To prepare the current probes for other applications. In view of the good results, the current probes could be used beyond the field of aeronautics. An example would be

for calibration of a surge generator. Nevertheless, a procedure of calibration should be described and the uncertainty budget of the system should be analyzed in order to be applicable as a metrological element to be used in laboratory.

5.3 Publications

A paper concerning the design of the test fixture with the title "*Design and validation of a test fixture for studying RF current flux through mechanical aircraft joints*" was presented at the "*2022 ESA workshop on aerospace EMC*" meeting of the European Space Agency on May 25th, 2022.

Currently, we are working on submitting a contribution to the journal "*IEEE Transactions on Electromagnetic Compatibility*" about the design, validation and calibration of current probes based on Rogowski Coils.

References

[1] Jose Pissolato Filho et al. "The effects of lightning currents in aircraft cfc structures". In: *IEEE Electromagnetic Compatibility Magazine* 10.1 (2021), pp. 62–69.

[2] SLJ Millen and Adrian Murphy. "Modelling and analysis of simulated lightning strike tests: A review". In: *Composite Structures* 274 (2021), p. 114347.

[3] N Muot et al. "Numerical evaluation of the lightning currents flowing through aircrafts fasteners–Comparison and cross-validation of methods". In: *2020 International Symposium on Electromagnetic Compatibility-EMC EUROPE*. IEEE. 2020, pp. 1–8.

[4] Yafei Shi et al. "A Review of Traditional Helical to Recent Miniaturized Printed Circuit Board Rogowski Coils for Power-Electronic Applications". In: *IEEE Transactions on Power Electronics* 35 (2020), pp. 12207–12222.

[5] Chucheng Xiao et al. "An overview of integratable current sensor technologies". In: *38th IAS Annual Meeting on Conference Record of the Industry Applications Conference, 2003.* Vol. 2. 2003, 1251–1258 vol.2. DOI: 10.1109/IAS.2003.1257710.

[6] Ayob Nazmy Nanyan et al. "The rogowski coil sensor in high current application: A review". In: *IOP Conference Series: Materials Science and Engineering*. Vol. 318. 1. IOP Publishing. 2018, p. 012054.

[7] Philipp Ziegler et al. "Wide Bandwidth Current Sensor for Commutation Current Measurement in Fast Switching Power Electronics". In: *2020 22nd European Conference on Power Electronics and Applications (EPE'20 ECCE Europe)*. 2020, P.1–P.9. DOI: 10.23919/EPE20ECCEEurope43536.2020.9215686.

[8] Mohammad Hamed Samimi et al. "The Rogowski coil principles and applications: A review". In: *IEEE Sensors Journal* 15.2 (2014), pp. 651–658.

[9] Helmut L Votzi, Markus Vogelsberger, and Hans Ertl. "Low-cost current sensor for power capacitors based on a PCB Rogowski-coil". In: *Proceedings of International Exhibition and Conference for Power Electronics, Intelligent Motion and Power Quality (PCIM Europe)*. 2011, pp. 621–626.

[10] Guillermo Robles, Muhammad Shafiq, and Juan Manuel Martınez-Tarifa. "Designing a Rogowski coil with particle swarm optimization". In: *Multidisciplinary Digital Publishing Institute Proceedings*. Vol. 4. 1. 2018, p. 10.

[11] M Shafiq et al. "Effect of terminating resistance on high frequency behaviour of Rogowski coil for transient measurements". In: *Elektronika ir Elektrotechnika* 19.7 (2013), pp. 22–28.

[12] J Zhu et al. "The design of Rogowski coil with wide band using for partial discharge measurements". In: *Proceedings of 2005 International Symposium on Electrical Insulating Materials, 2005.(ISEIM 2005).* Vol. 2. IEEE. 2005, pp. 518–521.

[13] Thomas Guillod et al. "Design of a PCB Rogowski Coil based on the PEEC Method". In: *2012 7th International Conference on Integrated Power Electronics Systems (CIPS).* IEEE. 2012, pp. 1–6.

[14] Zhou Li et al. "Design of Rogowski coil with external integrator for measurement of lightning current up to 400 kA". In: *Przeglad Elektrotechniczny* 87.7 (2011), pp. 188–192.

[15] Peerawut Yutthagowith. "Rogowski coil with a non-inverting integrator used for impulse current measurement in high-voltage tests". In: *Electric Power Systems Research* 139 (2016), pp. 101–108.

[16] Qinghua Tan et al. "Design of Open-Ended Structure Wideband PCB Rogowski Coil Based on New Winding Method". In: *Electronics* 11.3 (2022), p. 381.

[17] Jan Niklas Fritz, Christoph Neeb, and Rik W De Doncker. *A PCB integrated differential Rogowski coil for non-intrusive current measurement featuring high bandwidth and dv/dt immunity.* 2015.

[18] Esmaeil Hemmati and S Mohammad Shahrtash. "Evaluation of unshielded Rogowski coil for measuring partial discharge signals". In: *2012 11th International Conference on Environment and Electrical Engineering.* IEEE. 2012, pp. 434–439.

[19] Anna Eydan et al. "Design and fabrication of an optimized Rogowski coil for plasma current sensing and the operation confidence of Alvand tokamak". In: *Nuclear Engineering and Technology* 52.11 (2020), pp. 2535–2542.

[20] *CISPR 16-1-4:2019 (Ed. 4). Specification for radio disturbance and immunity measuring apparatus and methods - Part 1-4: Radio disturbance and immunity measuring apparatus - Antennas and test sites for radiated disturbance measurements.* Standard. Geneva, CH: Comité International Spécial des Perturbations Radioélectriques, Jan. 2019.

[21] Masanori Tsukuda et al. "Micro PCB Rogowski coil for current monitoring and protection of high voltage power modules". In: *Microelectronics Reliability* 64 (2016), pp. 479–483.

[22] Yadong Liu et al. “A novel transient fault current sensor based on the PCB Rogowski coil for overhead transmission lines”. In: *Sensors* 16.5 (2016), p. 742.

[23] Chris Hewson and Joanne Aberdeen. “An improved Rogowski coil configuration for a high speed, compact current sensor with high immunity to voltage transients”. In: *2018 IEEE Applied Power Electronics Conference and Exposition (APEC)*. IEEE. 2018, pp. 571–578.

[24] Ui-Jin Kim, Min-Soo Song, and Rae-Young Kim. “PCB-Based Current Sensor Design for Sensing Switch Current of a Nonmodular GaN Power Semiconductor”. In: *Energies* 13.19 (2020), p. 5161.

[25] *IEC 61000-4-5:2014. Electromagnetic compatibility (EMC) - Part 4-5: Testing and measurement techniques - Surge immunity test*. Standard. Geneva, CH: IEC (International Electrotechnical Commission), May 2014.

[26] Mathworks (2022). *cumtrapz - Cumulative trapezoidal numerical integration (R2022a)*. URL: `https://mathworks.com/help/matlab/ref/cumtrapz.html` (visited on 06/09/2022).

[27] *Lightning surge discharge design for SMPS applications - Line filter design guidelines with focus on CoolMOS™ P7*. AN_2006_PL52_2009_103328. V 1.0. Infineon Technologies. Aug. 2020.

[28] PSCad. *Standard Surge Waveforms*. URL: `https://www.pscad.com/webhelp/Master_Library_Models/CSMF/Surge_Generators/Wavelet_Transformation_(WT).htm` (visited on 05/09/2022).

[29] J De Freitas (2022). *MATLAB Central File Exchange. The DC Blocking Filter*. URL: `https://mathworks.com/matlabcentral/fileexchange/13792-the-dc-blocking-filter` (visited on 05/10/2022).

[30] KV Puglia. “Electromagnetic simulation of some common balun structures”. In: *IEEE microwave magazine* 3.3 (2002), pp. 56–61.

Appendices

A Circuital model of the implemented fixture

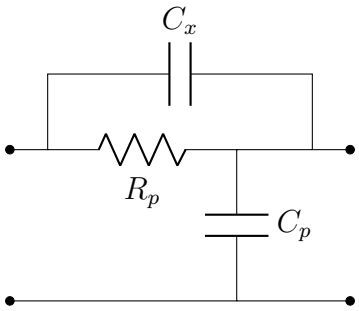

Figure 54: Circuital model of the single PCB trace.

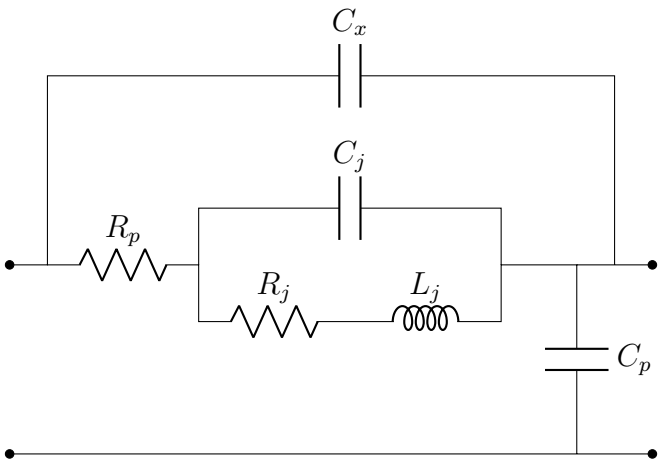

Figure 55: Circuital model of the fixture.

Where each element stands for:

- R_{p}: Resistance of the inner copper planes.
- C_{p}: Capacitance between inner conductor planes and GND reference plane.
- C_{x}: Parasitic capacitance between input and output ports.
- R_{j}: Metallic junction resistance.
- L_{j}: Metallic junction inductance.
- C_{j}: Metallic junction capacitance.

B Surge waveform characterization and simulation

A mathematical expression of the surge due to a direct lightning strike can be very useful when performing studies on this field, as it helps us to analyze various scenarios theoretically and by simulation [27]. The standard waveform for the surge can be expressed in terms of the following equation:

$$I(t) = k(e^{-\alpha t} - e^{-\beta t}) \tag{17}$$

Where α, β and k are constants that depend on the surge waveform used. Typical waveforms defined on the standard IEC 61000-4-5 are found on the following table [28]:

Waveform	Time constants	α	β	k
1.2/50 µs	$T_f = 1.67 \cdot T = 1.2\,\mu s$ $T_t = T_w = 50\,\mu s$	$1.45 \cdot 10^4$	$2.8353 \cdot 10^6$	1.0328
8/20 µs	$T_f = 1.25 \cdot T_r = 8\,\mu s$ $T_t = 1.18 \cdot T_w = 20\,\mu s$	$1.732 \cdot 10^5$	$8.66 \cdot 10^4$	-4

Table 5: Standard commonly used surge waveforms

Waveform name stands for the wavefront time (T_f) and the wavetail time (T_t). The wavefront time is defined usually as the rise time multiplied by a factor, that depends of how this rise time is defined. If it is defined from 10% - 90%, this factor is 1.67. If it is defined from 30% - 90% the factor is 1.25. Wavetail time is defined as the time when the current waveform reaches half of its maximum value. Usually, the 1.2/50 µs signal is associated to the open circuit output voltage of a surge generator and the 8/20 µs signal corresponds to the short circuit output current [25]. A zoomed surge waveform with the time constants used is illustrated in Figure 56.

Furthermore, take into account that Equation 17 provides a waveform that contains a DC component. In real conditions, this DC current does not exist, which means that the signal has to be filtered. If the signal is reproduced by a generator, it automatically filters out the DC component. However, in our application, if we need to reproduce the exact waveform, a DC-Block must be emulated [29]. The easiest way to do this is to employ an IIR filter with a cutoff frequency of 8 kHz.

Find illustrated in Figure 57 both simulated and already filtered signals. If we check the waveforms in the IEC 61000-4-5 standards we can verify that they exactly correspond to those presented.

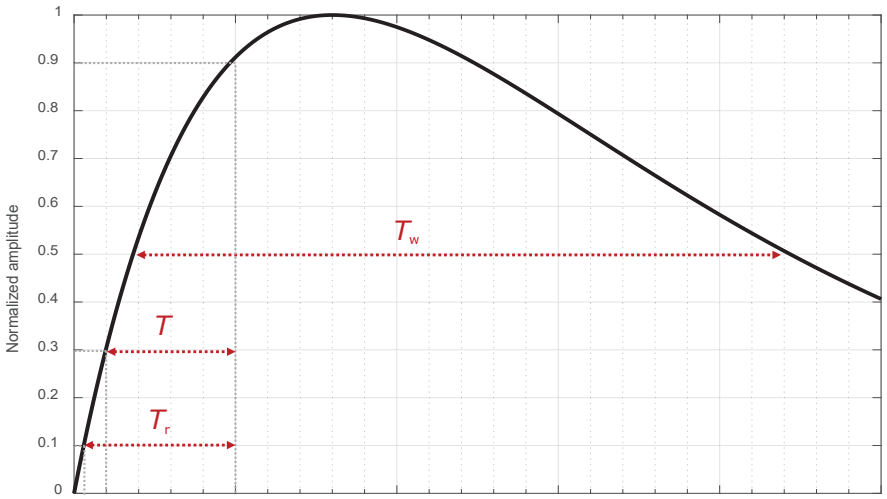

Figure 56: Zoomed surge waveform.

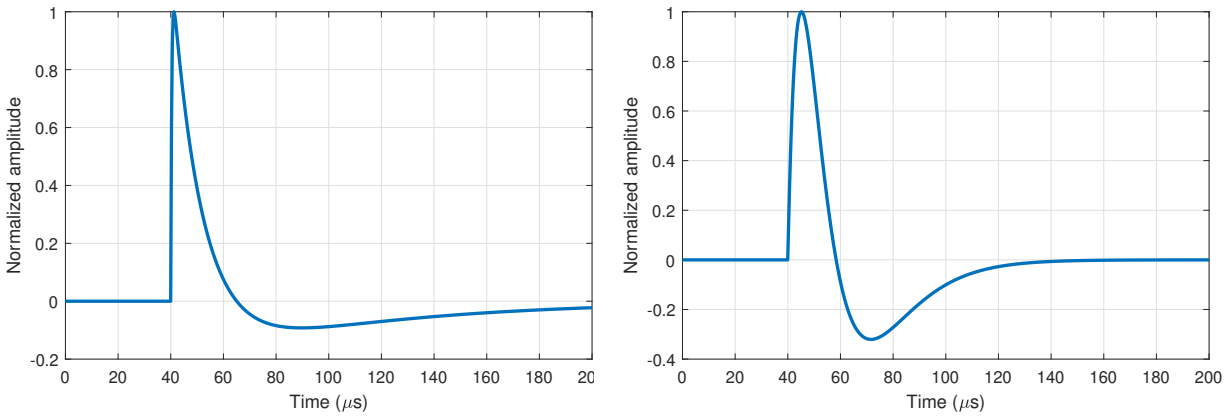

(a) 1.2/50 µs.

(b) 8/20 µs.

Figure 57: Simulated surge waveforms.

C Short overview of RF transformers and baluns

RF transformers as well as baluns are widely used in many applications such as microwave communications, radar, instrumentation, etc. Despite the fact that they are very similar elements (same construction, circuit diagram symbol easily confused), they have different operational characteristics and purposes, which sometimes might overlap.

The word "balun" is an acronym for "balanced-to-unbalanced". As the name indicates, it converts a differential or balanced signal with potentials equal to GND but with reverse polarity, to a single-ended signal, i.e. a signal that is referenced to GND. Baluns are typically used in RF systems such as antennas or mixers [30].

An RF transformer is identical to a conventional transformer but oriented to high frequency applications. It can be used to transform and/or isolate the voltage or current between different coupled circuits.

In our work, we will be using a broadband transformer to isolate the signal (transformer role) and at the same time convert a differential signal to a single-ended signal (balun role), so both terms have been alternated throughout the work. Many transformer topologies exist: with two terminals on each side only, three terminals, etc. In this annex we will see the simplest model, with just two terminals per side:

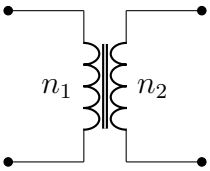

Figure 58: Symbol of a RF transformer.

Where n_1 is the number of turns of the primary winding and n_2 the number of turns of the secondary winding. The ratio between both values is a known value, since it allows to establish the relationship between voltage, current and impedance across both ports of the transformer. In this work we have used *Coilcraft PWB2010LB* transformer, which offers a bandwidth from to 3.5 kHz - 125 MHz. Turns ratio is 1:1, which indicates that the voltage and current are identical at the primary port and at the secondary port. The impedance seen from the primary port, therefore, is the same as the impedance of the secondary port.

In Figure 59 we can view the interior of the transformer used. We can observe that the cable is winded around a toroidal core which carries the magnetic flux between the primary and secondary winding. It is a structure similar to a common mode choke. Remark that the transformer has a very small size (6 mm per side) and can be integrated easily on a PCB.

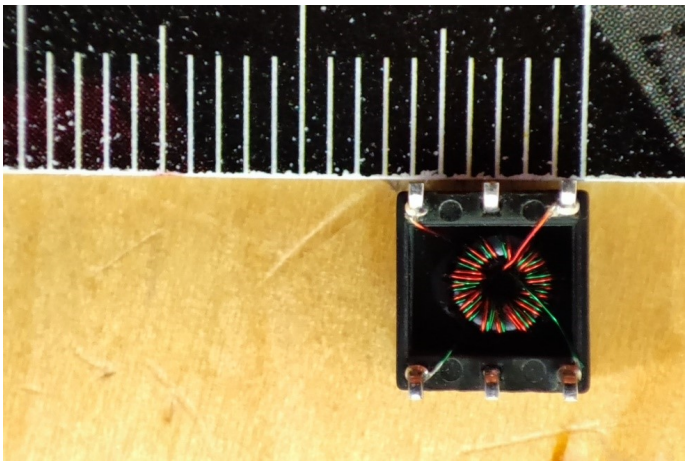

Figure 59: Interior view of a RF transformer.

In order to experimentally test the transformer, an evaluation board is designed (electronic schematic in Figure 60 and manufactured PCB in Figure 61). Different footprints are implemented in order to add components that could be included in the Rogowski coils and thus be evaluated if necessary. In this case, series elements ($R_{int,1}$ and $R_{int,2}$) have been short circuited and parallel elements (R_d and $C_{int,1}$) have been left open circuited.

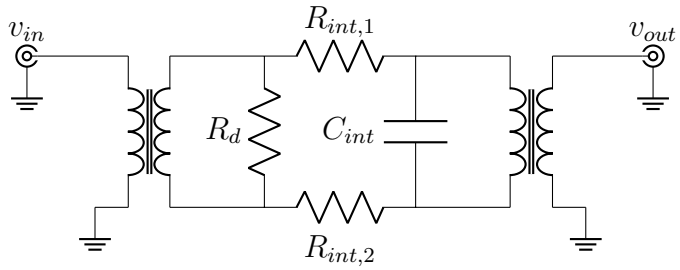

Figure 60: Circuit schematic of the transformer evaluation board.

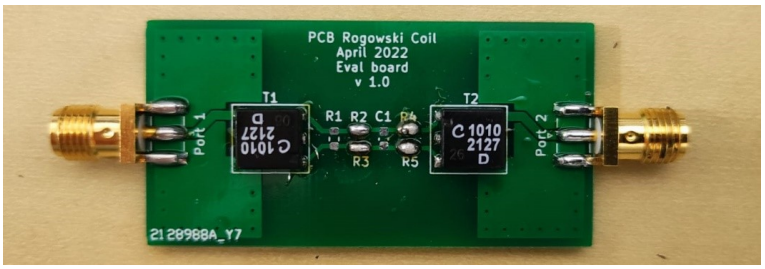

Figure 61: Manufactured PCB of the transformer evaluation board.

As a last step, the *Rohde&Schwarz ZVRE* VNA is used to evaluate the attenuation offered by the board (in this case parameter S_{21}) in the range from 10 kHz to 200 MHz:

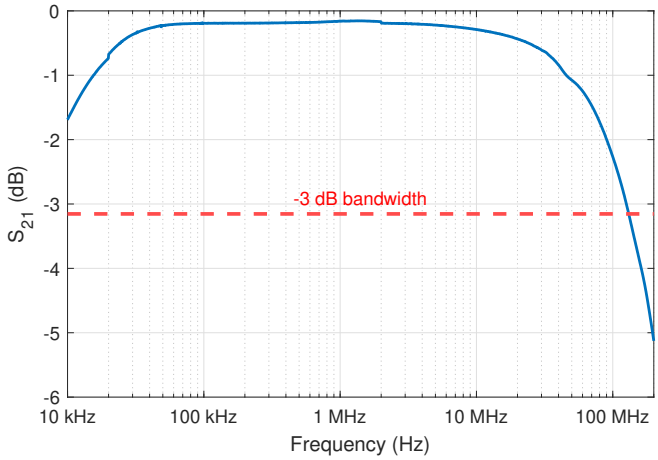

Figure 62: Attenuation offered by the transformer evaluation board.

It is seen that results obtained are within the specifications offered by the manufacturer. Although we cannot verify the minimum frequency of the bandwidth due to limitations of the measuring instrument, we can verify that in the upper part of the range the specification is fulfilled. In addition, in the range defined in this work (10 kHz - 10 MHz), there is a flat attenuation of approximately 0.4 dB (0.2 dB per transformer), so it would not be necessary to compensate or consider the transformer during normal operation.